Max-Planck-Institut für Meteorologie

REPORT No. 207

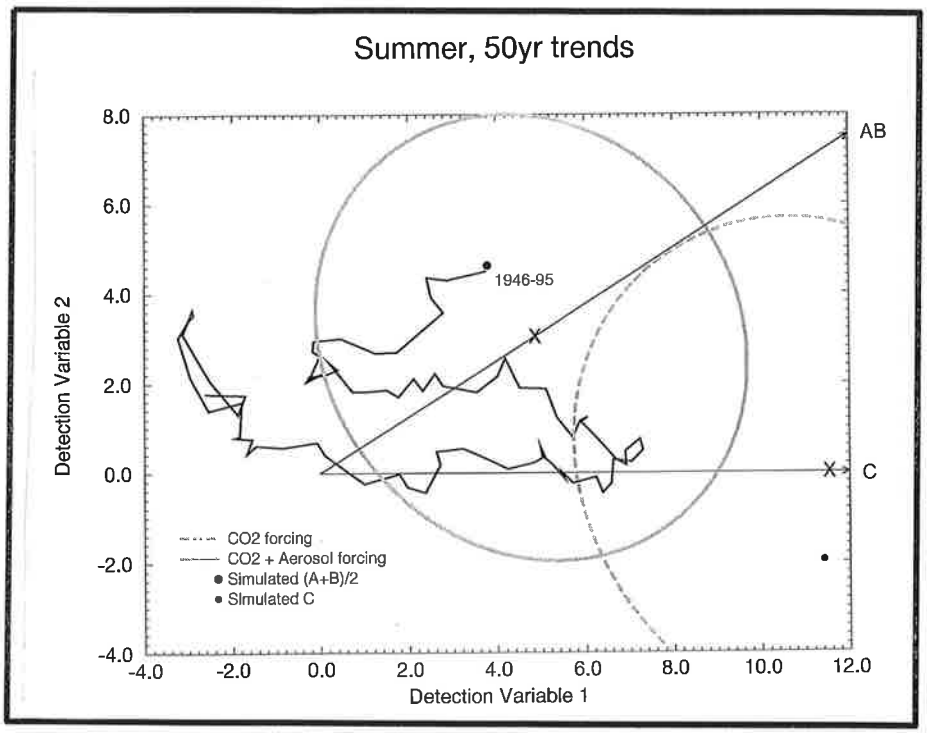

ON MULTI-FINGERPRINT DETECTION AND ATTRIBUTION OF GREENHOUSE GAS- AND AEROSOL FORCED CLIMATE CHANGE

by

Gabriele C. Hegerl • Klaus Hasselmann • Ulrich Cubasch
John F. B. Mitchell • Erich Roeckner • Reinhard Voss • Jürgen Waszkewitz

HAMBURG, July 1996

ISSN 0937-1060

AUTHORS:

Gabriele C. Hegerl
Klaus Hasselmann
Erich Roeckner

Max-Planck-Institut
für Meteorologie

Ulrich Cubasch
Reinhard Voss
Jürgen Waszkewitz

DKRZ
Deutsches Klimarechenzentrum
Bundesstr. 55
20146 Hamburg
Germany

John F. B. Mitchell

Hadley Centre
for Climate Prediction and Research
London Road
Bracknell, Berkshire
RG 12 257
Great Britain

MAX-PLANCK-INSTITUT
FÜR METEOROLOGIE
BUNDESSTRASSE 55
D - 20146 HAMBURG
GERMANY

Tel.: +49-(0)40-4 11 73-0
Telefax: +49-(0)40-4 11 73-298
E-Mail: <name> @ dkrz.de

On multi-fingerprint detection and attribution of greenhouse gas- and aerosol forced climate change.

GABRIELE C. HEGERL[1], KLAUS HASSELMANN[1], ULRICH CUBASCH[2], JOHN F.B. MITCHELL[3], ERICH ROECKNER[1], REINHARD VOSS[2] AND JÜRGEN WASZKEWITZ.[2]

1: Max-Planck-Institut für Meteorologie, Hamburg, Germany

2: Deutsches Klimarechenzentrum, Hamburg, Germany

3: Hadley Centre for Climate Prediction and Research, Bracknell, UK.

Corresponding Author address:

Gabriele Hegerl,
Max-Planck-Institut für Meteorologie,
Bundesstr. 55, 20146 Hamburg, Germany
email: hegerl@dkrz.de
fax: +49-40-41173 298
tel: +49-40-41173 309

ISSN 0937-1060

ABSTRACT

A multi-fingerprint analysis is applied to the detection and attribution of anthropogenic climate change. While a single fingerprint, as applied in a previous paper by Hegerl et al. (1996), is optimal for detecting a significant climate change, the simultaneous use of several fingerprints allows one to investigate additionally the consistency between observations and model predicted climate change signals for competing candidate forcing mechanisms. Thus the multi-fingerprint method is a particularly useful technique for attributing an observed climate change to a proposed cause.

Different model-predicted climate change signals are derived from three global warming simulations for the period 1880 to 2049. In one simulation, the forcing was by greenhouse gases only, while in the remaining two simulations the influence of aerosols was also included. The two dominant climate change signals derived from these simulations are optimized statistically by weighting the model-predicted climate change pattern towards low-noise directions. These optimized fingerprints are then applied to observed near surface temperature trends. The space-time structure of natural climate variability (needed to determine the signal-to-noise ratio) is estimated from several multi-century control simulations with different CGCMs and from instrumental data over the last 134 years.

Applying the combined greenhouse gas and aerosol fingerprint in the same way as the greenhouse gas only fingerprint in the previous paper, the recent 30-year trends (1966-1995) of annual mean near surface temperature are again found to represent a significant climate change at the 97.5% confidence level. Using both the greenhouse gas and the combined forcing fingerprints in a two-pattern analysis, a substantially better agreement between observations and prediction is found in terms of both spatial pattern and amplitude for the combined forcing simulation. The contribution of the aerosol forcing pattern to the greenhouse warming pattern can be detected at the

90% confidence level in the observations relative to most (but not all) estimates of climate variability.

The strongest influence of the aerosol component is found in longer term temperature trends in summer. The latest observed 50-year trend pattern of summer temperature is consistent with the greenhouse gas plus aerosol simulation with respect to both the pattern and the amplitude of the signal, while the observations are inconsistent with the greenhouse-gas only climate change signal at a 95% confidence level for all estimates of climate variability. Thus the two pattern analysis, in contrast to the single pattern analysis, is capable of distinguishing between the two forcing hypotheses in the observed climate change signal.

The results are subject to uncertainties associated with the model's climate change signal (for example, only the direct component of the aerosol forcing was considered) and the estimates of climate noise, which vary for different model control simulations. Further plausible mechanisms of climate change, e.g. changes in solar radiation or other anthropogenic forcing factors, also need to be investigated to clearly attribute the observed climate change to the anthropogenic forcing. Despite these uncertainties, we consider our results sufficiently robust to have some confidence in our finding that the observed climate change is consistent with the combined greenhouse gas and aerosol simulation, but inconsistent with greenhouse gas forcing alone.

1. Introduction

Since the beginning of industrialization, the concentration of greenhouse gases and anthropogenic aerosols in the atmosphere has continuously increased. There is considerable debate whether the global warming observed during this period can be distinguished from natural climate variability and whether the climate change signal, if detected, can be attributed to anthropogenic forcing. Estimates of natural climate variability based on a box upwelling-diffusion model of the ocean driven by stochastic forcing (Wigley and Raper, 1990) and long simulations with realistic coupled ocean-atmosphere general circulation models (CGCMs; Stouffer et al., 1994)) indicate that the observed 100-year trend of global mean temperature is larger than can be explained by the variability of these simulations. Applying information on the space-time structure of the greenhouse gas signal and the natural climate variability in an optimal fingerprint method, Hegerl et al. (1996) showed that the latest observed 20- and 30- year temperature trend patterns lie above the 95% significance level of current estimates of natural variability. It has been shown by Santer et al. (1995a) that the inclusion of aerosols enhances the agreement between observed and simulated global temperature patterns in summer and autumn and yields statistically significant trends in pattern correlation in these seasons with respect to climate variability estimates from unforced control simulations. The inclusion of aerosols also enhanced the pattern correlation of simulated and observed decadal mean temperature patterns (Mitchell et al., 1995a). A general agreement between observations and simulations has also been found for tropospheric temperature changes (Santer et al., 1996b). Thus there exists substantial evidence for a forced climate change in the last decades. A comprehensive summary of the findings of recent pattern-based detection studies is given in the 1995 IPCC Working Group 1 Second Assessment report (Santer et al., 1996a).

Nevertheless, it is pointed out in the IPCC report that while a high similarity of observed and simulated patterns suggests that the climate change has indeed been caused by the simulated anthropogenic forcing mechanisms, similar patterns can in principle also be

caused by other candidate forcing mechanisms in combination with natural climate variability. Thus the attribution problem requires that all relevant candidate forcing mechanisms be considered simultaneously.

To investigate the consistency of the observed climate change with model predictions for different candidate forcing mechanisms we apply here a multi-fingerprint analysis technique. We follow the optimal multi-fingerprint method of Hasselmann (1979; 1993; Hasselmann 1996) in which each of the fingerprints is statistically optimized by rotating the signal pattern away from regions of high natural variability towards low noise directions. The optimization is introduced to maximize the signal-to-noise ratio in estimating the contribution from different climate change signals to the observations, but is not a basic prerequisite of the attribution approach.

As observed climate data we take the near surface temperature data set of Jones and Briffa (1992). We apply a simplified form of the general space-time dependent optimal fingerprint method in which the optimization of the signal guess-patterns is carried out with respect to spatial coordinates only. To describe the time-evolution of the climate change signal we consider multi-decadal linear trends. By focussing on shorter time intervals, rather than the more traditional 100 year temperature increase, we make use of the fact that most transient CGCM simulations, which allow for a warming delay due to the heat uptake by the oceans, yield a marked enhancement of the warming rate in recent decades (Hasselmann et al., 1995, Cubasch et al., 1995, Mitchell et al., 1995a). This expected warming acceleration can be identified better by using relatively short temperature trends, e.g. over 30 years (Hegerl et al., 1996). Somewhat longer trends, e.g. over 50 years, are more useful for distinguishing a sulfate aerosol signal from the background noise, since the global mean sulfate burden has been increasing nearly linearly over the last 40 to 50 years (see also Santer et al., 1996b). The analysis of shorter time intervals has the additional advantage that the relevant level of natural variability can be estimated with higher confidence from model control simulations and observations.

We consider two climate change signals derived from new simulations forced either with greenhouse gases alone or with greenhouse gases and aerosols. A single fingerprint detection analysis using the combined greenhouse gas and aerosol signal applied to observed 30-year temperature trend patterns yields very similar results to those of Hegerl et al. (1996), who used a greenhouse gas only fingerprint (derived from an earlier climate model). The similarities in the results, despite differences in the forcing patterns, are due to the fact that for a single fingerprint the response is dominated by the global mean temperature increase, and reflects only to a small extent spatial details of the pattern (Santer et al., 1993; 1995a, Hegerl et al., 1996). However, applying the multi-pattern optimal fingerprint method, we find that the observations - in contrast to the single-pattern analysis- are no longer consistent with greenhouse gas forced climate change alone, while they are consistent with a combined greenhouse gas and aerosol forcing. Thus the application of two fingerprints permits a distinction between the two forcing mechanisms in the observations.

The attribution of climate change to a given cause is subject to more uncertainties than the more straightforward detection of climate change (Santer et al., 1996a). The candidate mechanisms need to be specified, together with the magnitude and statistical uncertainty of the forcing (in the case of sulfate aerosol forcing, for example, there is still high uncertainty regarding the magnitude and pattern of the forcing). The climate response to these forcings must be computed with climate models, which introduces uncertainties due to possible systematic model errors, while further uncertainties are associated with the estimate of natural climate variability. Also, the proposed method is based on the assumption that the different mechanisms can be superimposed linearly without interacting with each other and with climate variability. This linear superposition principle is essential if the response to combinations of forcing and variability is to be specified. Fortunately, there are indications that this is an acceptable approximation, at least for the greenhouse gas and aerosol forcing response (cf. Santer et al., 1995). As pointed out in Hegerl et al. (1996), the predicted climate change patterns need not be correct for detection: an incorrect pat-

tern merely reduces the power of the detection test, but will not normally lead to false detection claims. However, for attribution, model errors could lead to an incorrect assessment of the consistency between climate change simulations and observations, and even to an unjustified attribution claim. In principle, this problem can be addressed by considering possible systematic model errors. However, this has not been attempted, since the relevant model error covariance matrix for decadal trends is difficult to estimate.

The paper is structured as follows: Section 2 outlines the optimal fingerprint method for detection and attribution of climate change. In Section 3, the results of the greenhouse gas and aerosol simulations are given and the data used for the application of the detection and attribution approach are specified. Results for annual mean data are given in Sections 4 and 5, using one or two fingerprints, respectively, to test the consistency of the observed climate change with the hypothesized forcing mechanisms. A similar analysis for seasonally stratified data is presented in Section 6. The paper concludes with a summary and discussion of the results in Section 7.

2. The optimal fingerprint method for detection and attribution

Various pattern analysis methods have been proposed which make use of the model-predicted patterns of anthropogenic (or other externally forced) climate change to distinguish the forced signal from natural climate variability (noise) (cf. reviews in Barnett et al., 1991 and Hegerl and North, 1996). The optimal fingerprint method (Hasselmann et al., 1979; 1993) adopted here is based on an enhancement of features of the climate change signal associated with low natural variability relative to features which are more strongly contaminated by noise. Such techniques which maximize the signal-to-noise ratio are considerably more powerful than the selection of arbitrary climate indices (e.g. the global mean temperature) as detection variable, but require knowledge of the space-time structures of both the signal and the noise. This approach is useful not only for the early detec-

tion of externally forced climate change, but also for distinguishing between different candidate forcing mechanisms in the attribution problem (Hasselmann, 1996). The optimal fingerprint method has been applied by Santer et al. (1995b) for the detection of ocean global warming in a model simulation study and by Hegerl et al. (1996) for the detection of a greenhouse warming signal in near surface temperature data. It can be shown that the optimal fingerprint method is closely related to other optimal averaging or filtering methods (Bell, 1986; North et al., 1995; Hegerl and North, 1996) which provide an optimal estimate of the amplitude of a climate change signal in the presence of noise, and to similar approaches which have been used in other fields of signal processing (Hasselmann, 1979).

a. Optimal fingerprints

Observations of recent climate evolution may contain several climate change signals, e.g. through greenhouse warming, increasing aerosol concentrations, or changes in solar irradiance. To distinguish between different candidate mechanisms, it is useful to introduce several fingerprints $\underset{\sim}{f}_\nu = \left(f_\nu^i\right), \nu = 1 \ldots p$ associated with the different signal guess-patterns $\underset{\sim}{g}_\nu$ predicted for the different forcings, and to consider a vector of detection variables defined by the scalar products (Hasselmann 1993, Hasselmann, 1996)

$$d_\nu = f_\nu^i \Psi_i \qquad ,\nu = 1 \ldots p \tag{1}$$

where $\underset{\sim}{\Psi} = (\Psi_i)_{i=1\ldots n}$ represents the observed climate state vector (in some n-dimensional, e.g. gridpoint, space) and the summation convention is used for repeated indices. The optimal fingerprints are defined such that they maximize the square signal-to-noise ratio for each individual signal component. This yields at the same time the maximal multi-variate signal-to-noise ratio for the combined multi-pattern signal. For optimal detection (disregarding the question of attribution) the restriction to a single fingerprint generally yields the highest signal-to-noise ratio, since the significance of a given climate change signal decreases with increasing dimension (e.g. Hasselmann, 1993). The optimal

fingerprints are given by the product of the original signal guess-pattern with the inverse C^{ij} of the covariance matrix $C_{ij} = \langle \tilde{\Psi}_i \tilde{\Psi}_k \rangle$ of the random climate noise $\tilde{\Psi}$,

$$f_{\nu}^{i} = C^{ij} g_{\nu j}, \tag{2}$$

where the cornered brackets denote the statistical expectation. The fingerprint f_{ν}^{i} represents the contravariant dual vector of the covariant signal pattern vector $g_{\nu i}$, defined with respect to the metric C^{ij}.

The covariance matrix C_{ij} can be estimated using samples of model-derived or observed climate noise $\tilde{\Psi}$ (see below). The multiplication with the inverse covariance matrix C^{ij} suppresses features of the signal pattern associated with high natural variability and enhances pattern features for which the variability is low. This is seen most readily in the EOF representation $C_{ij} = diag\left(\sigma_i^2\right)$, for which the fingerprint is obtained by simply dividing the EOF coefficients of the signal pattern by the variance of climate noise σ_i^2. Detection is said to be achieved at some prescribed significance level p (e.g. 95%) if the "null" hypothesis that the observed detection variable d (or vector of detection variables) can be explained by natural variability alone is rejected at that significance level, i.e. if the probability that a signal of at least the estimated magnitude is sampled from the natural variability ensemble lies below the level 1-p (e.g. 5%).

b. Application of multiple optimal fingerprints to the attribution problem

The rejection of the null hypothesis does not yet attribute the observed climate change to the assumed generating mechanism. The detection test determines only whether the magnitude of the detection variable, defined with respect to some assumed signal direction, is too large to be explained by natural variability. It does not test whether the observations are in fact consistent with the model predicted signal, or with other model simulations using different forcing hypothesis (e.g. greenhouse gases alone, greenhouse gases and aerosols, solar insolation changes and so forth). This test is the essence of the attribution problem.

To test the consistency of a detected climate change signal with the signal predicted by a model we need to represent the observed climate change signal in terms of the model signal patterns g_ν, $\nu = 1, 2, \ldots p$:

$$\Psi_i = a^\nu g_{\nu i} + \tilde{\Psi}^r_i . \tag{3}$$

where $\tilde{\Psi}^r_i$ is a residual and we have used the summation convention again for the index ν. If all external forcing has been taken properly into account by the signal patterns, $\tilde{\Psi}^r_i$ will consist of climate noise only. The estimated signal pattern amplitudes a^ν can be expected to consist generally of linear combinations of the detection variables d_ν. However, since the detection components $d = (d_\nu)_{\nu = 1 \ldots p}$ were defined through equs.(1), (2) as the variables which maximize the signal-to-noise ratio for a detection test, they cannot immediately be equated with the amplitudes of the signal patterns. The p-dimensional amplitude vector $\boldsymbol{a} = \left(a^\nu \right)_{\nu = 1 \ldots p}$ is obtained from the condition that the mean square residual $\tilde{\Psi}^r_i$, defined with respect to the metric C^{ij}, is minimized:

$$C^{ij} \tilde{\Psi}^r{}_i \tilde{\Psi}^r{}_j = min \tag{4}$$

Minimizing the mean square residual with respect to the inverse covariance metric is equivalent to maximizing the probability that the residual represents a realization of the natural variability noise and does not contain signal components. The least square fit yields as determining equations for the signal amplitudes of the observed climate state $\underline{\Psi}$ (Hasselmann, 1996)

$$G_{\nu\mu} a^\nu = C^{ij} g_{\mu i} \Psi_j = d_\mu \tag{5}$$

where

$$G_{\nu\mu} = g_{\nu i} C^{ij} \cdot g_{\mu j} = f^i_\nu C_{ij} \cdot f^j_\mu . \tag{6}$$

If the signal patterns are statistically orthogonal (relative to the noise covariance matrix) and are furthermore normalized such that $G_{\nu\mu}$ is the unit matrix $I_{\nu\mu} = diag\,(1)$, the

detection variable components are statistically uncorrelated and yield the amplitude estimate directly: $a^{\nu} = d_{\nu}$ (in non-invariant notation for this particular representation).

c. Estimation of confidence intervals for the attribution test

For the attribution test, the observations and the model simulations are intercompared in terms of their respective signal vectors $\boldsymbol{a} = \left(a^{\nu}\right)_{\nu = 1...p}$, specifying the amplitudes of the climate change patterns g_{ν}. Since both the observed and the model simulated signal vectors are subject to uncertainties associated with climate noise and / or model errors, these uncertainties need to be specified in order to assess the statistical significance of deviations between the model and observed signal.

The uncertainty of the model predicted climate change signal consists generally of two contributions:

1) The uncertainty associated with the estimate of the climate change signal derived from a single (or a few) model simulations. A single simulation is subject to model-generated climate variability which contaminates the signal estimate (Cubasch et al., 1994).

2) The uncertainty associated with systematic model errors, ideally characterized by some model error covariance matrix. For the signal patterns used in this paper, these uncertainties are discussed in Section 3. The errors are difficult to estimate quantitatively, and we shall not include them in our statistical test. However, they need to be kept in mind when interpreting the results.

In principle, the first uncertainty can be removed by carrying out a large number of simulations, starting from different initial conditions, and forming the ensemble average. However, this is not feasible due to computer time limitations. Thus, the imperfect model estimated climate change signal $\boldsymbol{a}_M = \left(a_M^{\nu}\right)_{\nu = 1...p}$ will differ from the "true" (unknown) model predicted climate change signal by a sampling error governed by the statistics of the model's natural variability. If the superimposed climate variability is Gaus-

sian (the assumption of Gaussian distributions for the detection variable is discussed in Hegerl et al., 1996), the model climate change signal derived from a single simulation $\boldsymbol{y}$ represents a realization from a Gaussian distribution $\boldsymbol{y} \sim N(\boldsymbol{a}_M, \Sigma_M)$ where Σ_M denotes the model noise covariance matrix in the p-dimensional space spanned by the different climate change signals. (The signal uncertainty will also extend into the remaining dimensions of climate phase space, but these dimensions are irrelevant for the problem of distinguishing between a given finite set of p candidate forcing mechanisms.) Since we assume that the noise is superimposed linearly on the climate change signal, Σ_M can be inferred from the variations in the signal estimate due to noise only, which can be computed from a long control simulation using the same climate model. If the model predicted amplitude estimate is computed from the average of N different simulations Σ_M, is reduced by the factor 1/N.

Similarly, the estimated climate change signal of the observations will deviate from the "true" underlying climate change signal $\boldsymbol{a}_{obs} = \left(a_{obs}^{\nu} \right)_{\nu = 1 \ldots p}$ through the superimposed internal variability of the climate system. The signal vector inferred from the observations $\boldsymbol{x}$ will then also originate from a normal distribution $\boldsymbol{x} \sim N(\boldsymbol{a}_{obs}, \Sigma_{obs})$. If the climate model simulates the internal variability noise correctly, and the same method of inferring the signal pattern from the climate time series is applied to both the observed and the model simulated climate data, Σ_M would equal Σ_{obs}. In fact, neither condition is exactly satisfied, as will be discussed further in Section 5.

Both uncertainties are now combined for the attribution test:

We make the hypothesis that the model predicted climate change signal (or combination of signals) is correct. In this case $\boldsymbol{a}_{obs} = \boldsymbol{a}_M$, and the probability distribution of the difference vector $\boldsymbol{x} - \boldsymbol{y}$ between the observations $\boldsymbol{x}$ and model simulation $\boldsymbol{y}$ is given by the normal distribution

$$\boldsymbol{x} - \boldsymbol{y} \sim N(\boldsymbol{0}, \Sigma_{obs} + \Sigma_M) = N(\boldsymbol{0}, \Sigma) . \tag{7}$$

where we can set $\Sigma = \Sigma_{obs} + \Sigma_M$, since the noise realizations of the model and the observations are independent. From the distribution equ. (7) we can define ellipsoids of constant probability density containing, say, 90% of the realizations of the difference vector $\boldsymbol{x} - \boldsymbol{y}$ (cf. von Storch and Zwiers, 1996). If the model simulated climate change signal disagrees significantly from the observations, i.e. is not contained in the 90% uncertainty ellipsoid, the associated forcing mechanism is rejected as a plausible cause for the observed climate change signal at the 90% confidence level. Conversely, if the difference vector $\boldsymbol{x} - \boldsymbol{y}$ lies within this ellipsoid, the observations are considered to be statistically consistent with the postulated forcing mechanism - or sum of forcing mechanisms. A more rigorous terminology would be to say in this case that the observations are not inconsistent with the postulated forcing. However, we shall use the simpler but less precise wording given above.

3. Components of the detection and attribution approach

This Section describes the data used for implementing the multi-pattern detection and attribution approach: the observed data, the new simulations forced with greenhouse gases and aerosols, the signal-guess patterns derived from these simulations and the data for natural climate variability. We mostly focus on annual mean values. The generalization to seasonal values is described in Section 6.

a. Observations

The observed near surface temperature data used for the multi-fingerprint approach have been compiled as anomalies (with respect to the average of the years 1950-1979) of monthly mean near surface temperature on a 5° x 5° global grid by Jones and Briffa (1992) and Jones (1994 a,b). The data range from the year 1854 to 1995, with data coverage changing in time. Global-mean near-surface temperature curves and the decadal mean pattern of temperature change based on these data are presented in the Supplementary Report to the IPCC Working Group 1 Scientific Assessment (Folland et al. 1992). This

observed dataset is very similar to the newer, updated dataset used in IPCC 1995 (Nicholls et al., 1996). As in Hegerl et al. (1996), annual mean values at a gridbox were computed if at least one seasonal mean (computed from at least one month) was available, otherwise the annual mean was indicated as missing. This criterion allows a relatively high spatial coverage, but may introduce some additional noise. It corresponds to the criterion applied to the computation of decadal mean patterns in Folland et al. (1992). Our results were found to be insensitive to the criterion (e.g. use of a stricter acceptance condition of at least three seasonal means for an annual average). In the computation of averages of simulated and observed data and in the subsequent multi-fingerprint analysis, we considered only gridpoints for which the observations permit the computation of multi-decadal trends after 1949 such that not more than one year is missing between any two years with data (cf. Hegerl et al., 1996). This yields approximately 75% global coverage for annual mean data (cf. Figure 4). 30-year trend patterns computed in this manner are shown in Hegerl et al. (1996).

b. Greenhouse gas and aerosol simulations

The temperature change patterns for greenhouse gas only and combined greenhouse gas and aerosol forcing are derived from three climate change simulations with the coupled ocean atmosphere model ECHAM3+LSG, in the following referred to as HAM3L (Hasselmann et al., 1995; Voss et al., 1996). The model is a new version of the Hamburg CGCM (Cubasch et al, 1992; Maier-Reimer et al, 1993; Roeckner et al, 1992) using an updated atmosphere model (ECHAM3) at a spectral T21 resolution. The experiments start with forcing conditions of the year 1880 and are continued up to the year 2049. Two simulations (A and B) were carried out for a combination of both greenhouse gas forcing and the direct (albedo) effect of sulphate aerosols, while in the third simulation (C), only the greenhouse gas forcing was considered. The two aerosol plus greenhouse gas simulations differ only through the introduction of a small perturbation (at least an order of magnitude smaller than the uncertainty in the aerosol forcing, cf. Penner et al., 1995) into the aerosol

fields of one of the runs. Using more than one simulation enables a better separation of the climate change signal from the internal climate variability (evident in the independent fluctuations of the two simulations).

The greenhouse gas concentrations were expressed in terms of net equivalent CO_2 concentrations (Houghton et al., 1990). From 1880 to the present these were reconstructed from direct measurements since 1957 and, prior to that date, from estimates derived from ice cores (Schönwiese et al, 1990, Houghton et al., 1990). For the future, the IPCC Scenario A data were used (Houghton et al., 1990). The aerosol data were kindly made available by the Meteorological Institute of the Stockholm University and were calculated using the MOGUNTIA sulphur model (Langner and Rohde, 1991) from historical SO_2 emissions, based essentially on Mylona (1993) and Gschwandtner et al. (1986), and from projected future emissions from the IPCC 1992 scenario A (Pepper et al, 1992). The resulting global anthropogenic sulphur emissions increase from 10 Tg/yr in 1900 to 151 Tg/yr in 2050.

The scenario forcing fields are similar to those shown in Mitchell et al. (1995a,b), except that the pattern of the aerosol forcing was not spatially fixed before 1990, but was allowed to respond to the spatially changing patterns of sulfur emissions (see Mitchell and Johns, 1996). The impact of the computed aerosol concentrations was represented in the CGCM as an increased effective surface albedo. The global mean of the forcing at the top of the atmosphere due to the aerosols is approximately -0.7 W/m^2 in 1980. Indirect effects of aerosols on the formation and radiative properties of clouds were not considered. These are generally estimated to be of comparable magnitude to the direct effects, so that our computations of the aerosol climate impact must be regarded as only qualitative. Recent results indicate that the spatial pattern of climate change caused by indirect aerosol forcing may be different from that caused by direct forcing (Jones et al., 1994; Boucher and Lohmann, 1995).

Figure 1 shows the time evolution of the averages (over the analysis area covered by observations) of near surface temperature in the three experiments A, B, C, together with the observations. In all comparisons with observations, temperature change patterns are computed relative to the mean over the reference period 1950-1979 used in the observations. The residual drift of the control simulation may influence the time evolution to some extent (cf. below), especially in the early part of the simulation. The observed and simulated curves follow each other rather closely until about 1975, indicating that the aerosol effect had little influence on global mean temperature until then. From 1975 onwards, the greenhouse gas only experiment C shows a temperature rise of about 0.3 K per decade, compared to only 0.2 K per decade for the aerosol experiments A and B.

Figures 2 and 3 show the regional distribution of changes in northern hemispheric summer and winter temperature for the simulations without (a) and with inclusion of the aerosol forcing (b). The aerosols show the largest effects in the northern hemisphere, where the main sources of the aerosols are located. This hemisphere also shows the strongest seasonal signal. The impact of the aerosol forcing is generally larger in summer than in winter, and in low-and mid-latitudes, where the albedo effect is more effective due to the stronger insolation. However, the ice-albedo feedback enhances the signal in high latitudes in winter (Mitchell et al., 1995b).

A noteworthy feature is the impact of the aerosols on the Indian monsoon circulation. Without aerosols, most models predict a reinforcement of the monsoon (Gates et al., 1992; Kattenberg et al., 1996), while the aerosol experiment indicates instead a decrease in the strength of the monsoon and decreased rainfall. This is caused by the aerosol induced local cooling over Southern Asia, particularly over the Tibetan plateau (Lal et al, 1995; Mitchell and Johns, 1996).

c. Signal patterns of the model predicted climate change

For the detection and attribution analysis we need to define characteristic climate change patterns for the greenhouse gas only and the greenhouse gas plus aerosol simulations. We use two signal patterns $\underline{g}_v$ and associated fingerprints $\underline{f}_v$: one for the greenhouse gas only signal $\underline{g}_c$ and one for the combined greenhouse gas and aerosol signal $\underline{g}_{ab}$. It has been shown by Cubasch et al. (1992) that in the case of greenhouse gas forcing, the first EOF (empirical orthogonal function) captures most of the model response. Accordingly we define the temperature change patterns as the first EOF of the model response for each forcing experiment. This proved to be a better choice in the present case than the previous definition in terms of the difference pattern between the last and an early decade of the simulation (Hegerl et al., 1996), since the time averaging involved in the computation of the EOF reduced the noise contamination of the signal. This was helpful particularly for the combined forcing simulations, for which the climate change signal is smaller compared to noise than for the greenhouse gas only simulation. The difference between both choices (first EOF versus difference pattern) is small for the greenhouse gas only signal. The EOFs are computed from anomalies relative to the average over the model years 1950-1979 (i.e. relative to the reference period used in the observations) and only over areas with sufficient observational coverage. This ensures that the EOFs are defined for the same areas which are used later for detection.

The first EOF of simulation C yields a very stable representation of the annual mean climate change signal, explaining about 90% of the time evolution (Fig. 4a). To enhance the signal-to-noise ratio, the signal pattern (Figure 4b) for the greenhouse gas plus aerosol simulations A, B was determined from the first EOF of the mean of both simulations (A+B)/2. The signal pattern is rather similar to the greenhouse gas climate change signal except in the northern mid-latitudes, where the warming is reduced due to the aerosol effect. The full signal pattern correlation (including the spatial mean) for the EOFs of simulations (A+B)/2 and C is r=0.93, while the reduced correlation, after subtraction of the

spatial mean, is r*=0.32 (r and r* correspond to uncentered and centered pattern correlation in Santer et al., 1993). As expected, averaging both aerosol simulations substantially increases the variance explained by the climate change signal: The first EOF of (A+B)/2 explains 73% of the variance of (A+B)/2, whereas the first EOF of simulation A, for example, explains only 59% of the variance in A (the explained variance for the individual greenhouse gas plus aerosol simulations is smaller than for the greenhouse gas only simulation C because the climate change signal is smaller).

As in greenhouse gas only simulations the first EOF captures most of the time-evolution of the combined greenhouse gas plus aerosol climate change signal (Figure 5). The remaining EOFs show no systematic trends in the model years after ca. 1980 and have the appearance of noise. This result is confirmed by the computed 30-year trends of the principal components (not shown). Nevertheless, in the case of the greenhouse gas plus aerosol simulation, where the aerosol forcing pattern varies in time, some spatial details of the climate change pattern predicted for the present are necessarily distorted through the use of the first EOF of the entire simulation as time invariant signal pattern. Thus the strong cooling over China in the first EOF, Fig. 4b, is governed largely by the strong increase in aerosol forcing predicted in the IPCC scenario for the next century. Unfortunately, a more reliable computation of the present-day climate change signal would require a larger number of climate change simulations than is presently feasible (note that n simulations reduce the noise by a factor of only $n^{-1/2}$).

Some uncertainty is introduced by a drift in the HAM3L model. The drift appears to originate in the ice edge area of the Southern Hemisphere and causes a global mean warming of 0.5° C in 300 years in the unforced "control" simulation (CTL). Since we have computed the climate change pattern relative to a constant mean state (the average over the model years 1950-79), the slow warming trends in the first half of this century (Fig. 1) in the anomaly simulations A, B and C, and thereby also the signal pattern, could be influenced by a common model drift. However, the area in which the strongest drift occurs, the

high Southern latitudes, are not included in our signal guess-pattern (see Fig. 4). In order to qualitatively assess the effect of drift, we have also computed the first EOF of the climate change defined relative to the contemporal state of the control simulation (i.e. by subtracting CTL year by year from the climate change simulations, cf. discussion in Cubasch et al., 1992). The resulting time evolution of the first principal components after the model year 1970 is very similar in both cases. The first EOFs are also very similar, with a full pattern correlation of r=0.996 and a reduced pattern correlation of r*= 0.97. The differences between the pattern furthermore have the appearance of noise introduced by climate variability (not shown). We have used our original signal pattern definition, since subtracting the control simulation introduces additional climate variability from the control simulation into the climate change patterns, which causes problems in optimizing the fingerprint (Hegerl and North, 1996).

The Hadley Center simulations (Johns et al., 1996, Mitchell and Johns, 1996; Mitchell et al, 1995a,b, IPCC, 1996) yield similar rates of temperature increase to ours, both with and without aerosols, and quite similar spatial patterns. However, the responses to the two forcings separate about 20 years earlier in the Hadley Centre simulations. The climate change pattern of our new greenhouse warming simulation C shows a different pattern of warming over Europe and more pronounced warming over parts of the northern Hemisphere mid-latitude land masses than previous simulations using an earlier version of the Hamburg climate model (Cubasch et al., 1992; 1994a; 1994b). This may be attributed to a more realistic circulation, especially over the North Atlantic, in the updated atmosphere model ECHAM3 (Roeckner et al., 1992). However, the differences between the climate change signal of simulation C and the climate change signals of the earlier simulations (characterized by a reduced signal pattern correlation of r*=0.47 for the EIN simulation of Cubasch et al., 1994b, and r*=0.64 for the scenario A simulation of Cubasch et al., 1992) are still substantially smaller than the differences with respect to the combined greenhouse gas and aerosol simulation.

In summary, there are uncertainties of the signal pattern associated with: the initial residual drift of the control simulation; possible errors in the model response; the poorly known initial conditions in 1880; and the fact that a single greenhouse gas only simulation C and two greenhouse gas plus aerosol simulations are insufficient to separate details in the space-time evolution of the climate change signal reliably from the climate's internal variability (Cubasch et al., 1994). Still larger uncertainties arise from our present insufficient knowledge of the sulphate concentrations and, in particular, the resulting forcing (e.g. we have disregarded indirect aerosol forcing). We have also ignored other possible mechanisms of externally forced climate change, such as changes in ozone concentration, non-sulfate aerosols and land-surface changes. These shortcomings must be kept in mind in our later discussion of the attribution problem.

d. Data for natural climate variability

Estimates of the space-time structure of the natural near-surface temperature variability are needed for two purposes: to estimate the noise covariance matrix (equ. 2) for the computation of the optimal fingerprint; and to estimate the variability of the detection variable for computing significance levels for climate change detection and confidence ellipses for attribution. We use estimates which are based on four CGCM simulations of the present climate over several centuries: 1000 years from a simulation with the model ECHAM/LSG, referred in the following as HAML (v. Storch, 1994; v. Storch et al., 1996), a 1000 year simulation with the GFDL model (Manabe and Stouffer, 1993; 1996), 700 years with the model HAM3L, which has also been used for the climate change simulations, and 611 annual means from the control simulation with the HADCM2 model (Mitchell et al., 1995a, Johns et al., 1996; Tett et al., 1996). HAML has been used for a number of climate change simulations previously and is described in Cubasch et al. (1992). The HADCM2 model has a finer resolution of 2.5°latitude x 3.75° longitude than the other models.

In addition, the near surface temperature observations by Jones and Briffa (1992) are used to provide an estimate of the observed internal variability of climate, after subtraction of an estimate of the greenhouse gas signal as described in Hegerl et al. (1996). In the attribution approach, we use these data only as a yardstick for comparing some features of the model estimates of noise, since the observed time series is too short for the definition of reliable a two-dimensional confidence ellipses. Also, in contrast to the model control simulations, the observations may be contaminated by various naturally occurring or uncorrected anthropogenic external forcings (volcanic eruptions, changes in solar radiation, aerosol forcing, and a residual greenhouse gas signal due the imperfect representation of the subtracted signal, cf. Hegerl et al., 1996).

e. Construction of the optimal fingerprints

The noise covariance matrix used for constructing the optimized fingerprints from the signal patterns $\underline{g}_c$ and $\underline{g}_{ab}$ is estimated from 30-year trend patterns derived from the HAML simulation. The dimension of the full gridpoint space is too high to estimate the noise covariance matrix reliably from the limited amount of data. All data used in the detection and attribution analysis (i.e. the signal guess-patterns, the observed and all model trend patterns) are therefore truncated to a lower dimensional subspace. We chose the first 10 EOFs of the combined forcing simulation A. Using the average of the simulations A and B is not appropriate here since we wish to represent the climate noise, not average it out. Using the concatenated time series A, B rather than the single simulation A yielded essentially the same results. The climate change signals from both simulations $\underline{g}_c$ and $\underline{g}_{ab}$ were adequately represented in this space (to test this, the multi-fingerprint method using the non-optimized signal guess-patterns was performed both with and without truncation. The results were essentially identical in both cases). The truncation level was chosen prior to the detection and attribution analysis using the same considerations as in Hegerl et al. (1996). The choice is a compromise between

- retaining a sufficient number of degrees of freedom to represent the signal guess-patterns and rotate the patterns to obtain an optimized fingerprint and
- avoiding a rotation of the fingerprint into directions representing spurious small scale components with unrealistic low noise levels arising from inadequate sampling.

Small changes in the truncation level did not yield dramatically different results.

Figure 6 shows the optimal fingerprint for the combined greenhouse gas and aerosol forcing for annual mean near surface temperature (transformed back into gridpoint space). Compared to the original signal guess-pattern (Fig. 4b), the reduced warming south of Greenland is changed to a cooling extending into Northern Europe. The pattern over large land masses is also changed, for example over North America. The optimal fingerprint for the greenhouse gas only signal (not shown) shows substantially more warming in northern mid-latitudes than that for the combined forcing. Its spatial pattern resembles the optimal fingerprint based on the earlier EIN greenhouse warming pattern (Hegerl et al., 1996), for example in the cooling south of Greenland, but deviates in some minor spatial details.

4. Results for a single fingerprint

In the previous section we have introduced the basic components of the multi-pattern detection and attribution method, namely the observations, signal guess-patterns (represented by the first EOF of the simulations), the data for natural climate variability and the optimal fingerprints.

For the detection - as opposed to the attribution - of climate change, a single-pattern analysis, as used in Hegerl et al. (1996), is the most effective approach, since the power of a statistical test is highest for small dimensions (see e.g. Hasselmann 1979). We shall accordingly first carry out a single pattern detection analysis, applying the signal pattern from the combined greenhouse gas and aerosol forcing experiment (A+B)/2 in the same way as in the previous greenhouse warming detection study (Hegerl et al. 1996), to investigate

whether the modified signal pattern yields different results for detection. For that purpose we compute the detection variable equ. (1) from the observations, estimate the variability of the detection variable associated with natural climate variability and assess then the statistical significance of the recent 30-year trend. The results of each of these steps are shortly discussed in this Section. A more detailed discussion of assumptions and technical details is given in Hegerl et al. (1996). Subsequently, we shall apply both fingerprints derived from the different signal guess-patterns (Fig. 4) to address the attribution question and assess which of the two experiments - C or (A+B)/2 - is more consistent with the observations.

Figure 7 shows the time evolution of the computed detection variables $d(t)$ (equ. 1) obtained by applying the optimal fingerprint derived from the experiment (A+B)/2 to the spatial patterns of running 30-year trends $\Psi(t)$ computed from the observations (Jones and Briffa, 1992). The fingerprint is normalized to unity with respect to the HAML covariance matrix metric $f^i_{ab} C_{ij} \cdot f^j_{ab} = 1$. Thus the values of the detection variable are expressed in units of one standard deviation of the detection variable computed for the HAML noise (this may have a bias to small values since the noise has been used for computing the optimal fingerprint, cf. below, but this is irrelevant for our present discussion). Also shown in Figure 7 are the time evolutions of the detection variables obtained by applying the optimal fingerprint to running 30-year trends of the climate change simulations (A+B)/2 and C. The recent rapid increase in the detection variable for the observations agrees quite well with the time evolution of the detection variable computed from the various simulations, although there are differences in the timing. The detection variable for both simulations stabilizes at a constant level in the first half of the next century, indicating a constant rate of temperature increase at that time.

The time evolution of simulation C indicates an earlier warming compared to the combined forcing simulation (A+B)/2, but also compared to the earlier EIN greenhouse warming only simulation in Hegerl et al. (1996). While the first feature is expected due to the

aerosol forcing in the simulations A and B, the latter difference is presumably related to model differences and a retarded warming in the EIN simulation (which may be partly caused by a fluctuation or equilibration problem in the Northern Hemispheric sea ice in the first part of the EIN simulation, Cubasch et al., 1995).

Since both predicted signal patterns (Fig. 4) are dominated by the global mean warming contribution, the detection variable will also be dominated by the global mean warming trends (Santer et al., 1993; 1995a, Hegerl et al., 1996). This explains why the trends from simulation C are not strongly reduced although the signal pattern is different from the assumed combined forcing signal pattern. It also explains why the evolution of the detection variable computed with the observations and the combined forcing fingerprint is quite similar to the earlier results using a greenhouse warming only fingerprint. The distinction between the two detection variables is better seen using a two-pattern approach, as will be discussed in the next section.

In Figure 7, the detection variable for the latest observed trend (1966-1995) d computed with the optimal fingerprint f_{ab} for the combined forcing (fig. 6) is seen to exceed the 95% confidence intervals (discussed below) for climate noise, as estimated from CGCM simulations and from the observations. Since positive values of the detection variable are expected for anthropogenic climate change, the significance levels can be based on a one-sided test. For this test, the upper limits of the 95% confidence intervals in Figure 7 denote the 97.5% significance limits. Thus we conclude that the latest observed trend (1966 - 1995) exceeds the 97.5% significance level for an observed climate change signal for all estimates of natural variability, and that the null hypothesis that the observed temperature trends are natural can be rejected. The high level of the detection variable around 1945, representing the trend 1916-1945, may be explained as a superposition of an early greenhouse warming signal and an extreme natural variability event and is discussed further below.

The 95% confidence intervals have been estimated independently for each set of climate variability data and are based on the mean square variability $\langle \tilde{d}^2 \rangle$ of the detection variable d for 30-year trends computed from these data. The HAML simulation, which was used to estimate the covariance matrix C_{ij} used to construct the fingerprint, was excluded. Otherwise the non-independence of the optimized fingerprint and the data (Hegerl et al., 1996) would have yielded an artificially suppressed value. In estimating $\langle \tilde{d}^2 \rangle$ from observational data, gaps in the time series before 1949 were filled by a least-square regression. The estimates of the 95 % confidence intervals from the estimated variances of the different variability data sets were corrected for sampling bias of the relatively short time series using Monte Carlo simulations of a Gaussian first-order auto-regressive process with the same time series length and autocorrelation as the data (cf. Hegerl et al., 1996).

The observations yield higher variability levels than the coupled models, and the model estimates also differ among each other. However, the differences between observed and simulated variances are in fact smaller than the differences in the 95% confidence intervals shown in Figure 7. This is because the 95% confidence intervals, inferred from the Monte Carlo simulations, are approximately +/- 2.4 times the estimated standard deviation for the relatively short observed times series, as compared to approximately +/- 2.0 for the longer model simulations.

For a quantitative estimate of the benefit of using the optimal fingerprint method it is useful to consider the signal-to-noise ratio

$$s/n = \frac{d}{\langle \tilde{d}^2 \rangle^{1/2}} \tag{8}$$

for various alternative definitions of the detection variable. Table 1 lists the signal-to-noise ratios estimated from different sets of variability data and for three different definitions of the detection variable: (a) the global mean (uniform fingerprint); (b) the scalar product of the observations with the signal guess-pattern ($f = g$); and (c) the detection variable computed with the optimal fingerprint (equ. 2). The improvements in the estimated signal-to-

noise ratio for the latest observed trend using the signal guess-pattern as fingerprint relative to the straightforward global mean is on the order of 5% for most data, while the potential further improvement due to the use of the optimal fingerprint rather than the signal pattern depends strongly on the set of variability data used to estimate $\langle \tilde{d}^2 \rangle$. The standard deviation $\langle \tilde{d}^2 \rangle$ generally decreases when the optimal fingerprint is used (normalizing all fingerprints to the same mean square deviation), but as d may also decrease, the signal-to-noise ratio does not necessarily increase in all cases. For example, the standard deviation estimated from 30-year trends of the HADCM2 control simulation was only slightly smaller than that estimated from the observed variability data if the signal pattern was used as fingerprint, but the variability decreased more in the HADCM2 data than in the observations through use of the optimized fingerprint, leading to a stronger increase in signal-to-noise ratio for the HADCM2 data. On the other hand, using the GFDL variability *de*creased s/n marginally for the optimal fingerprint, while the HAM3L variability data yielded even lower s/n values for the optimized fingerprint.

The differences in the reduction in $\langle \tilde{d}^2 \rangle$ resulting from use of the same optimized fingerprint indicates that the structure of the variability on timescales of several decades is not consistent between different models. The full potential of the optimal fingerprint approach will presumably be realized only when the models are able to simulate the real climate variability with higher fidelity. However, we should keep in mind that a poor estimate of the noise covariance matrix leading to a "wrong" - i.e. not truly optimal - fingerprint will merely reduce the power of the detection method. This may result in the inability to detect a climate change signal which an accurate fingerprint would have detected, but it will not normally lead to an incorrect detection claim.

We conclude that the reliability of the estimated significance level of the latest observed trends is limited primarily by the reliability of the variability estimates. However, the high signal-to-noise ratios listed in Table 1 provide some cushion against the uncertainties in variability estimates, yielding some confidence in the positive detection result.

5. Towards attribution: Application of a two-pattern analysis

While it has been shown in the previous Section that the latest observed 30-year trend patterns indicate a statistically significant climate change, the cause of this change has not been clearly established. The high values of the detection variable are due mainly to a strong global mean warming, rather than a high similarity between the predicted and observed climate change patterns. Figure 8 shows the reduced pattern correlation r*(t) (after subtraction of the spatial mean) between the observed 30-year trend patterns and the model derived climate change patterns. The correlation with the signal pattern for the combined forcing rises to the order of 0.3 only for the latest few trend patterns (Fig. 8), in agreement with other results using seasonal and decadal mean data (Santer et al., 1995a; and Mitchell et al., 1995a). The reduced pattern correlation between the observed and greenhouse gas only signal pattern is smaller for the trends ending between 1970 and 1990, but of the same magnitude (~0.3) for the latest observed trends.

As described in Section 2, a multi-fingerprint method can be used to distinguish between different forcing mechanisms on a more quantitative basis. For that purpose, first the statistically orthogonal signal pattern to the greenhouse gas signal pattern is introduced. Both the greenhouse gas alone and the orthogonal, aerosol related, signal pattern are then used to determine if the introduction of the aerosol forcing significantly enhances the agreement between simulation and observations, and to investigate if the observations are consistent with either a combined greenhouse gas and aerosol forcing or with greenhouse warming alone.

a. Application of two fingerprints

Since the signal guess patterns of both forcing simulations exhibit a general qualitative similarity (fig. 4), the detection variables $d_c = f_c^{'} \cdot \Psi_i$, $d_{ab} = f_{ab}^{'} \cdot \Psi_i$ (equ. 1) computed with each fingerprint will be rather highly correlated.

The analysis and also the graphical presentation of results is simplified if orthogonal signal patterns and fingerprints (relative to the metric C^{ij}) are introduced. In this case the detection variables can be directly equated with the amplitude estimates (equs. 5, 6). As first signal pattern we use the greenhouse warming signal guess-pattern $g_{ci} = g_{1i}$ (normalized to unity with respect to the inverse covariance matrix, $g_{1i}C^{il}g_{1l} = 1$) and as second pattern the orthogonal pattern

$$g_{2i} = g_{abi} - \left(g_{abj}C^{jl}g_{1l}\right)g_{1i}, \tag{9}$$

or in terms of optimal fingerprints

$$f_2^i = f_{ab}^i - \left(f_{ab}^j C_{jl} f_1^l\right) f_1^i. \tag{10}$$

The second pattern then needs only to be normalized in the same way as the first. Figure 9b shows the optimal fingerprint f_2 for the statistically orthogonal signal-guess pattern (equ. 10, computed in the 10-dimensional truncated space, and then transformed back into gridpoint space for plotting). Figure 9a shows for comparison the spatial pattern derived from the combined forcing climate change pattern, orthogonalized (in the gridpoint space) to the greenhouse gas only climate change pattern (fig. 4a) using the Euclidean rather than the covariance metric. The latter pattern can be superimposed on the greenhouse warming signal pattern, Fig. 4a, point-by point to yield the combined greenhouse gas and aerosol signal pattern and thus represents directly the pattern contributed by the aerosol forcing. The zonally rather uniform cooling in the northern mid-latitudes in both patterns is caused by the zonal distribution of aerosols resulting from the sulfur emissions in this latitude band. The corresponding statistically orthogonal signal guess-pattern (equ. 9, not shown) also shows more cooling in the northern mid-latitudes.

Figure 10 a shows the evolution of the observed running 30-year trend patterns in the two-dimensional phase space spanned by the detection variables d_1 and d_2. In the ortho-normal pattern representation, each point in the phase space directly represents an amplitude estimate of the greenhouse gas only pattern ($a^1 = d_1$) and the orthogonal aerosol forcing

pattern ($a^2 = d_2$). The combined greenhouse gas plus aerosol climate change pattern can be expressed in terms of the patterns $g_{ci} = g_{1i}$ and the aerosol forcing pattern g_2 in the form:

$$g_{abj} = c_1 g_{1j} + c_2 g_{2j} \tag{11}$$

by computing the coordinates $c_\nu = g_{abi} C^{ij} g_{\nu j}$, $\nu = 1, 2$. The arrow C along the d_1 axis denotes the direction of the greenhouse-gas only signal ($d_2 = 0$) in Fig. 10a, while the arrow AB represents the direction of the greenhouse gas plus aerosol signal (as predicted by the model) $d_1/d_2 = c_1/c_2$.

Figure 10a indicates that the latest trend patterns, e.g. the trends 1948-77 until 1966-1995, generally agree more closely with the combined forcing climate change signal than with the greenhouse gas only signal. To judge the statistical significance of those results, the path of the detection variable of 30-year trend patterns is shown together with the corresponding climate noise data (Figure 10b) computed from 30-year trends for different model control simulations and for the observed variability data. The figure clarifies the relation between the different single-pattern detection results discussed previously (e.g. Figure 7). Projection of all data onto the direction AB yields the detection variable and noise distribution for the combined forcing signal pattern, while projection onto the direction C yields the corresponding result for the greenhouse gas only signal pattern. It is clear from a visual inspection that the detection results for both signal patterns will be rather similar, as the angle between the two pattern directions is rather small. A distinction between the two cases can be made only in the two-dimensional phase space.

Figure 10b indicates that the peak warming trends exceed the 95% confidence intervals of natural variability trends in all model control simulations not only in the last decades, but also in the first half of this century. The fact that the observations exceed the model noise level in this period implies that some caution is appropriate in interpreting our detection results (cf. also Barnett et al., 1996). However, the computed 30-year trends of a 570 year paleoclimatic record of summer mean temperatures over northern hemisphere land con-

firm that the warming in the early part of this century was indeed an unusual event, yielding the largest 30-year trend in the entire paleoclimatic record (Bradley et al., 1993). Some of this trend may represent an early anthropogenic signal. If an estimate of the greenhouse gas signal is subtracted from the observations (green dots "VOBS" in fig. 10c), the modified data lie substantially closer to the model internal variability domain. Furthermore, estimates of solar insolation changes indicate a possible increase in solar irradiance in that period (Hoyt and Schatten, 1993; Crowley and Kim, 1996). This suggests that the observed warming in the first half of this century was partly forced, partly an extreme event of internal climate variability. We cannot say from this evidence that the observed data suggest an inconsistency between model and observed internal climate variability.

Figure 10b also depicts the 95% confidence ellipses for two-dimensional Gaussian distributions fitted to the different sets of climate variability (the 90% confidence regions considered later are correspondingly smaller concentric ellipses). The bias due to sampling, which was estimated using Monte Carlo techniques in the one-dimensional detection test, has not been taken into account in the computation of the two-dimensional confidence areas. Thus we do not show estimates of the confidence ellipses for the relatively short observed time series. For the longer model time series (611 to 1000 years), the ellipsoids can be estimated with some confidence, and a cursory visual inspection suggests that a representation of the noise by a Gaussian distribution is an acceptable approximation. The differences in the noise distributions of the internal variability simulated by the different climate models are clearly larger than can be explained by sampling uncertainty.

b. Significance of the aerosol pattern contribution

We investigate now the consistency of the computed evolution of the detection vector for the alternative global warming simulations with the observed evolution. As a first test whether the inclusion of aerosols significantly improves the statistical agreement between the observations and the model climate change pattern we consider the signal-to-noise

ratio of the second (aerosol) component d_2 for the latest observed trend. If the signal-to-noise ratio is sufficiently high to reject the hypothesis that d_2 represents climate noise only, we conclude that there is a significant aerosol related pattern in the observations. This test is independent of the global mean warming which dominates the value of d_1. Since we wish to investigate the consistency of the observations with a greenhouse gas only signal pattern (corresponding to zero values of d_2), unusually high positive or negative signals are relevant. Thus two-sided confidence intervals, as opposed to the previous 1-sided test for single pattern detection, are used.

Table 2 shows that d_2 is larger than noise at the 90% confidence level if the estimate of climate variability is derived from the observations and from the GFDL control simulation, but it is insignificant at this confidence level relative to the HADCM2 and the HAM3L noise estimates. The sampling uncertainty in the confidence levels due to the finite length of the time series has been estimated using Monte Carlo simulations in the same way as for the detection confidence levels. The magnitude of the detection component d_2 in the latest observed trend pattern (and thus the outcome of the consistency test) is sensitive to technical details of the optimization procedure. If the scalar product between the (non-optimized) orthogonal signal pattern and the observations is used to compute d_2, the resulting value is insignificant relative to all estimates of climate variability (Table 2). The angle between signal patterns (expressed by the ratio c_2/c_1, equ. 11) varies with the truncation level and with the variability data used for estimating the covariance matrix. This implies uncertainties in the computation of the statistically orthogonal signal pattern (i.e. in the form of the ellipses, fig. 10b). Furthermore, even for the relatively stable c_2/c_1 values in Table 2, the value of d_2 is sensitive to the analysis parameters. We conclude from the relatively low signal-to-noise ratio, combined with these uncertainties, that the contribution of the aerosol pattern to the observed annual mean 30-year trend patterns cannot at present be convincingly distinguished from noise. However,

a more positive conclusion will be reached later when we consider longer time trends and seasonally stratified data.

c. Application of the attribution test

We turn now to the attribution method described in Section 2. Here the full two dimensional detection vector is considered to determine whether the observed climate change is consistent with the proposed forcing mechanisms. This involves assessing the difference between the detection vector computed from the most recent observed 30-year trends for the years 1966-1995 and the corresponding detection vector predicted by a model simulation using the given forcing mechanism. If the difference vector lies within a given confidence ellipse determined by the uncertainty in the estimates of the observed and model simulated detection vectors (equ. 6), the climate change is regarded as consistent (formally not inconsistent) with the proposed mechanism, otherwise the attribution test fails.

Figure 11 shows again the evolution of the detection variables for the observations in the d_1, d_2 phase space. The values of the simulated trends 1966-1995 are given by the red dot for the greenhouse gas only simulation C and the blue dot for the combined forcing simulation (A+B)/2. However, instead of using these model trend vectors directly, we prefer to project the detection vectors onto the directions of the signal pattern as defined by the EOFs of the full simulation (cf. Section 2). Projecting the vector corresponding to the blue dot onto the direction AB and the vector represented by the red dot onto the direction C, we obtain as model predicted vectors characterizing the climate change patterns the blue and red crosses X, respectively. We believe that this definition will provide more stable estimates of the model simulated signal vectors for the last thirty year trends, at least with respect to the signal directions. However, if the non-modified model trend vectors are used instead, the attribution analysis yields essentially the same results.

The covariance matrix Σ characterizing the confidence ellipse of the difference vector between the observed and model simulated trend signals is given by the sum of the covari-

ance matrix Σ_M of the statistical model signal uncertainty and the corresponding covariance matrix Σ_{obs} of the natural variability noise in the observations (Section 2, equ. 7). (The covariance matrix estimated from the HAM3L internal variability must be divided by two for the mean greenhouse gas plus aerosol simulation (A+B)/2 in order to allow for the reduction in uncertainty through averaging over two simulations.) Since the internal variability of the HADCM2 model yielded the largest ellipse (fig. 10b), we use this model as the most conservative of our estimates of natural climate variability.

Figure 11 shows the resulting confidence ellipses, centered on the model predicted signals for the latest 30 year trend (note the smaller ellipse for the combined forcing simulation representing the mean of two simulations). For the greenhouse warming only signal, the detection vector for the latest observed trend lies outside the 90% confidence ellipse. Thus the difference between the model-simulated and observed 1966-1995 trend is larger than can be explained by Gaussian noise at this confidence level. Nevertheless, the point still lies sufficiently close to the confidence ellipse that in view of the inherent uncertainties in estimating the natural climate variability and in determining the statistically orthogonal direction we cannot conclude with high confidence that the observations are indeed inconsistent with a pure greenhouse warming signal. On the other hand, the detection variable for the latest observed 30-year trends lies well within the 90% uncertainty ellipse for the combined forcing signal. Thus we conclude that the observations for the 30-year trends of annually averaged data agree well with a combined forcing signal pattern, but it cannot be concluded with high statistical significance that they are inconsistent with a climate change signal due to greenhouse gas forcing alone. This is in agreement with our previous conclusions based on the analysis of the single detection component d_2. To obtain a clearer separation of the aerosol and greenhouse gas signals, we therefore turn to seasonally stratified data and consider longer trend intervals.

6. Results for seasonally stratified data

As has been mentioned, 30-year trends were chosen for the analysis of the annual mean data in order to focus on the accelerating greenhouse warming predicted by climate models for the last decades. However, this choice is presumably not optimal for distinguishing between global warming due to greenhouse gases alone and greenhouse gas plus aerosol forcing. Aerosol forcing shows a pronounced increase over the last 50 years, and we therefore expect that 50-year trends should be more suitable for the attribution issue. This is indicated also by the results of Santer et al. (1995a), who found that in correlations of climate change patterns including the spatial mean, 30-year trends yield the strongest differentiation from natural variability noise, whereas if the spatial mean is removed (and thus the bulk of the warming signal), the residual observed spatial pattern correlates better with the predicted signal if longer trends are considered. Furthermore, the aerosol effect is expected to be strongest in summer. Thus we focus on 50-year trends in this season. Figure 12 shows the pattern of the latest observed 50-year trends for the period 1946-1995 for Northern Hemispheric summer, from the data of Jones and Briffa (1992). The reduced warming or cooling in the northern hemisphere is in qualitative agreement with the climate change pattern of the greenhouse gas plus aerosol model simulation (cf. Figure 3).

As in the case of annual mean values, the signal guess patterns for seasonal mean data are identified with the first EOFs computed from each transient global warming simulation. Generally, the area with acceptable data coverage is smaller (~ 66% of the earth surface) for seasonal data (a gridbox is accepted as yielding a seasonal datapoint if at least one month is observed) than for the annual mean data (~75%, as discussed in Section 3).

The strongest effect of aerosols is seen in the northern hemispheric summer and autumn (Fig. 3), as expected, whereas the winter pattern of the combined forcing simulation is similar to the greenhouse gas pattern except for a strong cooling over china (Fig. 2). This latter feature, as pointed out, is associated with strongly increasing sulfur emissions over China in the 21st century in the IPCC scenario. The first EOF of the average (A+B)/2 of

the two combined forcing simulations explains approximately 48% of the variance in winter and spring and 58% in summer and autumn, compared with 73% for the annual mean. The higher explained variance for the annual mean data is a consequence of the reduction of the natural variability noise through averaging over the annual cycle. For the greenhouse gas only simulation C, the first EOF explains about 80% of the variance in winter and spring and about 85% in summer and autumn, compared with 92% for the annual mean.

The time evolution of the EOF coefficients for seasonal data is very similar to the annual mean case (Fig. 5). Trends computed from the principal component time series confirm that for trends ending after about 1990, the first EOF captures most the climate change signals in all seasons, the higher EOFs having the appearance of noise with no clear trend. However, prior to this date, EOFs 2 or 3 pick up some of the cooling signal in the 1940ies to 1970ies, when the aerosol forcing was relatively strong compared with the still rather weak greenhouse forcing.

Prior to the use of 50-year trends in summer, seasonal mean 30-year trends have been analyzed for all seasons. The results confirm the previous annual mean results and are thus not given in detail: the observations indicate a positive but insignificant aerosol forcing pattern in all seasons but winter, and the amplitude of the aerosol related pattern cannot be rigorously distinguished from noise in any season. A rather interesting feature of the results using seasonally stratified data was that the robustness of the (single-pattern) detection variable results using the optimal fingerprint varied between seasons. Table 3 shows a comparison of the signal-to-noise variable for the detection variable computed from the (non-optimized) signal pattern together with the detection variable using the optimal fingerprint (equ. 1). Generally, the signal-to-noise ratio increases or remains approximately constant through optimization for nearly all variability data in summer and autumn. A slight decrease for the HAM3L and GFDL data no longer occurs if the truncation space is reduced to 8 dimensions. In contrast, the signal-to-noise ratio *de*creases for all data in win-

ter and spring. This is not altered by using a lower truncation level (e.g. 4 EOFs). It also occurs if the covariance matrix is estimated from different model control simulations, with the exception of the HADCM2 model (which features a higher resolution). This systematic decrease in the signal-to-noise ratio through optimization may be caused by incorrect signal guess-patterns, or by incorrect model noise. Possibly, the lower-resolution models have difficulty treating the strong cyclonic wave activity in winter.

For the detection and attribution analysis, the 50-year summer trends were analyzed in essentially the same way as the 30- year trends of the annual mean data. However, since the sampling uncertainties become larger when longer trends are considered, we augmented the original data from the HADCM2 control run by data from a recently completed extension of the simulation, yielding 976 realizations of each season. At the same time we truncated the representation to a 6-dimensional space prior to optimization rather than a 10-dimensional space, since the 1000 years of HAML data yield proportionally less independent 50-year trends than 30-year trends. Since the first 6 EOFs of the combined forcing simulation A were insufficient to represent the greenhouse gas only pattern (indicated, for example, by differences in the time evolution of the non-optimized detection variable before and after truncation), the 6th EOF was replaced by the first EOF of the greenhouse gas only simulation, thereby ensuring that the pattern was properly represented.

Table 4 lists the signal-to-noise ratios for the detection variable d_2 associated with the aerosol pattern. The most recent 50-year trend has a significantly higher d_2 component than any of the variability data at the 90% confidence level (even at the 95% confidence level for most data). Table 4 also shows that this result is not strongly dependent on the use of optimal fingerprints. The signal-to-noise ratio is nearly as high if the non-optimized signal guess-patterns are used to compute the detection variable. The results using optimal fingerprints show higher signal-to-noise ratios mainly because the fingerprints are more separated, as indicated by the higher ratios of c_2/c_1 (equ. 11).

A further analysis using data over land and ocean separately revealed that both land and ocean contribute to the statistical significance of the aerosol pattern. This can also be anticipated from Figure 3, which shows comparable aerosol induced cooling or reduced warming over both land and ocean in the northern mid-latitudes.

Figure 13a shows the evolution of the detection vector for the observed 50-year trends in summer in the two-pattern phase space, together with samples of the internal climate variability and the 95% confidence ellipses for different climate noise data. The sampling distribution again suggests that the use of a Gaussian distribution is justified. The most recent 50-year trend for summer shows a strong contribution of the aerosol related pattern (already shown in Table 4). This trend also deviates from all estimates of climate variability at the 95% confidence level. Figure 13a further indicates that the strong trends in the early part of this century agree slightly better with greenhouse warming than with combined forcing climate change. These trends are very unusual relative to the model internal noise samples. As discussed above, this is suggestive of a forced component or an exceptional event in the warming record in the early part of this century.

Figure 13 b shows the results of the attribution method for summer 50-year trend patterns. The 50-year trend patterns ending in 1995 derived from the greenhouse gas only and the combined forcing simulations are indicated by the red and blue dots, respectively, yielding the red and blue crosses after projection onto the respective signal patterns. As in the annual mean case, the results are not affected significantly if the model derived signal estimates are used directly rather than their projections in the direction of the EOF signal patterns. The 95% confidence ellipses for the vector representing the difference between the model and observed signals are computed in the same manner as for the annual mean data, using again the HADCM2 noise as an estimate of internal climate variability.

The latest observed 50-year summer trend pattern agrees surprisingly well with the model prediction for the greenhouse gas plus aerosol simulation, as indicated by the very small signal difference vector in this case. The difference vector lies well within the 90% - not

shown- and 95% confidence ellipse. In contrast, the observed trend pattern lies far outside the confidence ellipse of the greenhouse gas only forced climate change signal. The statistical results listed for the aerosol component d_2 in table 4 indicate that this statistical inconsistency is found even when only the contribution from the aerosol forcing is considered, disregarding the additional inconsistency arising from the higher predicted global warming component d_1 in the direction of the greenhouse gas only warming signal.

Our results are consistent with the results of Santer et al. (1995a). The authors found a slow increase in recent decades of the (reduced) pattern correlation between the observed and simulated summer and autumn near surface temperatures. The signal patterns were taken from an equilibrium coupled atmospheric-mixed layer ocean model simulation using in a greenhouse gas plus aerosol forcing.

In summary, we conclude that the latest (1946-1995) 50-year trend of observed near surface summer temperatures is statistically inconsistent with the greenhouse gas only forced climate change signal at a confidence level higher than 95%, and is highly consistent with the combined greenhouse gas and aerosol forcing simulation. In contrast to the less conclusive results from investigation of the annual mean 30 year trends, these conclusions are robust with respect to technical details of the analysis.

7. Discussion and conclusions

In a detection and attribution study of externally forced climate change, we have applied single and multi-fingerprint analyses to observed patterns of 30-year trends of annual mean and 50-year trends of summer near surface temperatures. The fingerprints are derived from three new model simulations, one forced with greenhouse gas forcing only, two with additional (direct) aerosol forcing. Using a single fingerprint derived from the average of the two greenhouse gas and aerosol forced climate change simulations, we confirm the result of the previous study of Hegerl et al. (1996) that the latest observed 30-year trend pattern of annual mean data, ending in 1995, can be distinguished from our estimates

of natural climate variability at a 97.5% significance level, i.e. the probability of observing a trend which yields values as high as the observed detection variable due to natural climate variability alone is less than 2.5%.

The latest observed warming trend agrees better, both in terms of pattern and amplitude, with a combined greenhouse gas and aerosol signal than with a greenhouse gas only signal. The distinction between the two forcing scenarios can best be studied in the phase space spanned by the two signal patterns. The two-pattern attribution analysis shows that the observed climate change is consistent with the combined greenhouse gas and aerosol forced signal computed with the HAM3L model for annual mean 30-year trends. It is even more consistent for the 50-year trends for (northern) summer, the season with the most pronounced aerosol impact.

On the other hand, the latest observed 30-year trend pattern is inconsistent at the 90% confidence level with the greenhouse gas only simulation. However, the confidence level of this inconsistency result is not high and subject to uncertainties associated with technical details of the analysis. In contrast, the latest 50-year trends of summer mean data are found to be inconsistent with greenhouse gas only forcing at the 95% confidence level. The inconsistency outcome of this test is not only more significant but also more robust with respect to modifications of the analysis.

Our investigations indicate that the most effective data filter is generally different for the detection problem, in which the goal is to distinguish between forced climate change and internal climate variability, and the attribution problem, in which the consistency of competing forcing mechanisms with an observed but noisy climate change signal is tested. The strongest and most stable signal for detection is found in the 30-year trends of annual mean data. This corresponds to the recent accelerated warming predicted by models. However, the largest difference between greenhouse gas and aerosol forced climate change appears in the 50-year trends in summer. This is consistent with the near linear

increase in aerosol forcing since the middle of this century and the stronger impact of aerosols on the radiation balance in the summer.

Our results are subject to uncertainties associated with the model-derived climate change signals. Possible systematic errors in the climate model, e.g. errors in the model sensitivity or arising from the residual model drift (whose effect is estimated as small, however) have not been taken explicitly into account. Although the good agreement between the climate change signals simulated by our model and the HADCM2 model (Mitchell et al., 1995a) gives some confidence in the signal patterns, uncertainties remain both in the form of the direct aerosol forcing and in the contribution from the indirect aerosol forcing. The latter has been ignored in our simulations but is estimated to be of comparable magnitude to the direct forcing.

However, the most critical aspect of our analysis are the uncertainties in the estimate of climate variability. The climate noise is inferred from observations (after subtraction of an estimate of the climate change signal) and from the internal variability of different CGCM control simulations. The impact of uncertainties in the natural variability estimates was most apparent in the analysis of the winter and spring seasonal data. The strong dependence of the results on the noise estimates of different models and the failure to systematically increase the signal-to-noise ratio through optimization suggest that the structure of the observed multi-decadal climate variability is not correctly reproduced by the different climate models in these seasons. These model divergences in the description of the natural climate variability create some uncertainties in the outcome of all detection and attribution strategies based on pattern oriented methods. The full potential of the optimal fingerprint method will not be realized before these uncertainties are resolved through further model improvements and intercomparison studies.

Nevertheless, the signal-to-noise ratio for our detection of a climate change signal in the annual mean 30-year temperature trends is quite high, and largely independent of the details of the optimization and the data used to estimate climate variability. Furthermore,

the statistical significance of the inconsistency of the greenhouse gas only signal with the observations found for the 50-year summer trends is also high and quite stable. Thus we have some confidence in our principal conclusions.

We remark finally that the present approach to the attribution of a detected significant climate change to different candidate mechanisms is necessarily limited to hypotheses which are specified a priori. Candidates other than the anthropogenic forcing by a pure greenhouse warming and a combined greenhouse gas and aerosol forcing should also be investigated, such as a change in solar radiation (e.g. Hoyt and Schatten, 1993; Crowley and Kim, 1996). However, although solar radiation changes may cause a similar pattern of near surface temperature change as an increase in greenhouse gases, the amplitude of the present climate change seems to be too high to be explained by the hypothesized changes in solar forcing alone (Cubasch et al., 1996).

Despite these caveats, we conclude from our analysis that the multi-fingerprint method is a useful quantitative approach for the attribution problem of deciding whether an observed climate change signal is consistent, at some prescribed confidence level, with one or a number of competing candidate forcing mechanisms. While a single-pattern analysis yields the result that a significant climate change has been observed which is consistent with either hypothesis of a pure greenhouse gas warming or a combined greenhouse gas plus aerosol forcing, we conclude from a two-pattern analysis that the observed climate change is inconsistent with greenhouse warming alone at a confidence level higher than 90%, while it is consistent with a combined greenhouse gas plus aerosol signal.

8. Acknowledgments

The authors are grateful to Hans von Storch for support in many aspects of this work, to Henning Rodhe for providing the aerosol forcing data and to Phil Jones for the latest near surface temperature data and for helpful discussions. We wish to also thank Ben Santer and Lennart Bengtsson for useful comments, Uli Schlese for providing the simulation

data, Simon Tett for assistance in the application of the HADCM2 control simulation and constructive discussions and Ron Stouffer for the GFDL simulation data. Marion Grunert drew the diagrams. The MPI simulations were carried out at the DKRZ. The work was sponsored by the Bundesministerium für Bildung, Wissenschaft, Forschung und Technologie (BMBF) through the contract „Klimavariabilität und Signalanalyse“, by the Max-Planck-Gesellschaft and by the EC Environmental Program under the contract No. ENV4-CT95-0102.

References

Barnett TP, Schlesinger ME and Jiang X (1991) On greenhouse gas detection strategies. In Greenhouse-Gas-Induced-Climatic Change: A Critical Appraisal of Simulations and Observations. M. E. Schlesinger ed., 537-558. Elsevier Science Publishers, Amsterdam.

Barnett, TP, Santer BD, Jones PD, Bradley RS and Briffa KR (1996): Estimates of low Frequency Natural Variability in Near-Surface Air Temperature. The Holocene, in press.

Bell TL, 1986: Theory of optimal weighting of data to detect climatic change. J. Atmos. Sci. 43, 1694-1710.

Boucher O, Lohmann U (1995) The sulfate-CCN-cloud albedo effect. A sensitivity study with two general circulation models. Tellus 47B: 281-300

Bradley RS and Jones PD (1993) 'Little Ice Age' summer temperature variations: their nature and relevance to recent global warming trends. The Holocene, 3, 367-376.

Briffa KR and Jones PD (1993) Global surface air temperature variations during the twentieth century: Part 2, implications for large-scale high-frequency palaeoclimatic studies. The Holocene, 3, 77-88.

Crowley TJ and Kim K-Y (1996): Comarison of proxy records of climate change and solar forcing. Geophys. Res. Letters., 23, 359-362.

Cubasch U, Hasselmann K, Höck H, Maier-Reimer E, Mikolajewicz U, Santer BD and Sausen R (1992) Time-dependent greenhouse warming computations with a coupled ocean-atmosphere model. Climate Dynamics, 8, 55-69.

Cubasch U, Santer BD, Hellbach A, Hegerl GC, Höck H, Maier-Reimer E, Mikolajewicz U, Stössel A and Voss R (1994) Monte Carlo climate forecasts with a global coupled ocean-atmosphere model. Climate Dynamics, 10, 1-19.

Cubasch U, Hegerl GC, Hellbach A, Höck H, Mikolajewicz Santer BD and Voss R (1995) A Climate change simulation starting from 1935. Climate Dynamics, 11, 71-84

Cubasch U, Hegerl GC, Voss R, Waszkewitz J, Crowley TJ (1996): Simulation with an O-AGCM of the influence of variations of the solar constant on the global climate. Submitted for publication.

Folland CK, Karl TR, Nicholls N, Nyenzi BS, Parker DE and KYa Vinnikov (1992): Observed climate variability and change, Section C, in Climate Change 1992. The supplementary report to the IPCC scientific assessment. Houghton J. T., B. A. Callander and S. K. Varney (eds.), 135-170. Cambridge University Press, Cambridge.

Gates WL, Mitchell JFB, Boer GJ, Cubasch U, Meleshko VP (1992): Climate Modelling, Climate Prediction and Model Validation. Climate change 1992. The supplementary report to the IPCC scientific assessment. Houghton J. T., B. A. Callander and S. K. Varney Eds, Cambridge University Press, Cambridge, 97-134.

Gschwandtner G, Gschwandtner K, Eldrige K, Mann C and Mobley D (1986) Historic Emissions of sulfur and nitrogen oxides in the United States from 1900 to 1980. J. Air Poll. Contr. Ass. 36, 139-149.

Hasselmann K (1979): On the signal-to-noise problem in atmospheric response studies. Meteorology Over the Tropical Oceans, D. B. Shaw, ed., Royal Meteorological Society, Bracknell, Berkshire, England, 251-259.

Hasselmann K (1993) Optimal fingerprints for the Detection of Time dependent Climate Change. J. Climate, 6, 1957-1971.

Hasselmann K (1996): Multi-pattern fingerprint method for detection and attribution of climate change. In preparation.

Hasselmann K., Bengtsson L, Cubasch U, Hegerl GC, Rodhe H, Roeckner E, von Storch H, Voss R, and Waszkewitz J (1995): Detection of anthropogenic climate change using a fingerprint method. MPI report, 168 and Proc. "Modern Dynamical Meteorology", Symposium in Honor of Aksel Wiin-Nielsen, 1995. ed. P. Ditlevsen (ECMWF press 1995), 203-221

Hegerl GC, von Storch, Hasselmann K, Santer BD, Cubasch U, and Jones PD (1996): Detecting Greenhouse Gas induced Climate Change with an Optimal Fingerprint Method. J. Climate, in press.

Hegerl GC and North GR (1996): Statistically optimal methods for detecting anthropogenic climate change. J. Climate, accepted.

Houghton JT, Jenkins GL and EphraumsJJ (eds.) (1990) Climate change. The IPCC Scientific Assessment. Cambridge University Press, Cambridge, 364 pp.

Houghton JT, CallanderBA and Varney SK (1992) Climate Change 1992. The supplementary report to the IPCC Scientific Assessment. Cambridge University Press, Cambridge, 200 pp.

Houghton JT, and Meira Filho LG1(1996) Climate Change 1995. The IPCC second scientific assessment. Cambridge University Press, Cambridge, 572pp.

Hoyt DV and Schatten KH, (1993): A discussion of plausible solar irradiance variations, 1700-1992. J. Geophys. Res., 98, 18895-18906.

Johns, TC, Carnell RE, Crossley JF, Gregory JM, Mitchell JFB, Senior CA, Tett SFB and Wood RA (1996): The second Hadley Centre Coupled Model:description, spinup and validation. Climate Dynamics, provisionally accepted.

Jones A, Roberts DL and Slingo A (1994): A climate model study of the indirect radiative forcing by anthropogenic aerosols. Nature 370, 450-453.

Jones PD (1994a) Recent warming in global temperature series. Geophys. Res.Lett., 21, 1149-1152.

Jones PD (1994b) Hemispheric Surface Air Temperature Variations: A Reananlysis and an Update to 1993. J. Climate., 7, 1794-1802.

Jones PD and Briffa KR (1992) Global surface air temperature variations during the twentieth century: Part 1, spatial, temporal and seasonal details. The Holocene, 2, 165-179.

Kattenberg A, Giorgi F, Grassl H, Meehl GA, Mitchell JFB, Stouffer R, Tokioka T, Weaver AJ, Wigley TML (1996) Climate Models - Projections of Future Climate. The IPCC Second Scientific Assessment. J. T. Houghton et al., ed. 285-357.

Lal M, Cubasch U, Voss R and Waszkewitz J (1996): The transient response of greenhouse gases and sulphate aerosols on monsoon climate. submitted to Climate Change.

Maier-Reimer E, Mikolajewicz U and Hasselmann K (1993) Mean circulation of the Hamburg LSG model and its sensitivity to the thermohaline surface forcing. J Phys. Oceanogr., 23, 731-757.

Manabe S and Stouffer RJ (1993): Century-scale effects of increased atmospheric CO_2 on the ocean-atmosphere system. Nature, 364, 215 - 218.

Manabe S und Stouffer RJ (1996) Low Frequency Variability of Surface Air Temperature in a 1000 year integration of a Coupled Ocean-Atmosphere Model. J. Climate, 9, 376-393.

Mitchell, JFB., Johns TJ, Gregory JM and Tett SFB (1995a) Transient climate response to increasing sulphate aerosols and greenhouse gases. Nature, 376, 501-504.

Mitchell, JFB., Davis RA, Ingram WJ and Senior CA (1995b) On surface temperature, greenhouse gases and aerosols, models and observations. J Climate, 10, 2364-3286.

Mitchell JFB and Johns TJ (1996) On the modification of greenhouse warming by sulphate aerosols. J . Climate, accepted.

Mylona S. (1993) Trends of sulphur dioxide emissions, air concentrations and depositions of sulphur in Europe since 1880. Report EMEP MSC-W no. 2/93, Norwegian Meteorological Instiaute, Oslo, Norway.

Nicholls, N., Gruza GV, Jouzel J, Karl TR, Ogallo LA, Parker DE (1996): Observed Climate Variability and Change; in: Houghton JT, and Meira Filho LG, 1996: Climate Change 1995. The IPCC second scientific assessment. Cambridge University Press, Cambridge, pp 133-192.

North GR, Kim K-Y, S. Shen SSP and Hardin JW (1995) Detection of Forced Climate Signals, Part I: Filter Theory. J. Climate 8, 401-408.

North GR and Kim K-Y, 1995: Detection of Forced Climate Signals, Part II: Simulation results. J. Climate 8, 409-417.

Parker, DE, Jones PD, Folland CK, and Bevan A, (1994): Interdecadal changes of surface temperature since the late nineteenth century. J. Geophys. Res., 99, 14373-14399.

Penner JE, R. J. Charlson, Hales JM, Laulainen NS, Leifer R, Novakov T, Ogred J, Radke LF, Schwartz SE and Travis L (1995): Quantifying and Minimizing the Uncertainty of Climate Forcing by Anthropogenic Aerosols, Bull. Am. Met. Soc., 75, 375-400.

Pepper W, Leggett J, Swanrt R, Wasson J, Edmonds J and Mintzer I (1992): Emission scenarios for the IPCC; An update - Assumptions, Methodology, and Results. Report to IPCC WG1 Secretariate, Bracknell, UK.

Roeckner E, Arpe K, Bengtsson L, Brinkop S, Dümenil L, Esch M, Kirk E, Lunkeit F, Ponater M, Rockel B, Sausen R, Schlese U, Schubert S, Windelband M (1992): Simula-

tion of the present-day climate with the ECHAM model: Impact of model physics and resolution. MPI report, 93.

Roeckner E, Siebert T, and Feichter J (1995): Climate response to anthropogenic sulfate forcing simulated with a general circulation model. In: Charlson, R., Heintzenberg, J. (eds). Aerosol Forcing of Climate.

Santer BD, Wigley TML and Jones PD, 1993: Correlation methods in fingerprint detection studies. Climate Dynamics, 8, 265-276.

Santer BD, Taylor KE, Penner JE , Wigley TML, Cubasch U, and Jones PD (1995a) Towards the detection and attribution of an anthropogenic effect on climate. Climate Dynamics, 12: 77-100.

Santer BD, Mikolajewicz U, Brüggemann W, Cubasch U, Hasselmann K, Höck H, , Maier-Reimer E, Wigley TML (1995b): Ocean variability and its influence on the detectability of greenhouse warming signals. J. Geophys. Res, 100, 10693-10725.

Santer BD, Wigley TML, Barnett TP, Anyamba E (1996a) Detection of climate change and attribution of causes. Climate change 1995. The IPCC Second Scientific Assessment. J. T. Houghton et al., ed. 407-444.

Santer BD, Taylor KE, Wigley TML, Jones PD, Karoly DJ, Mitchell JFB, Oort AH, Penner JE, Ramaswamy V, Schwarzkopf MD, Stouffer RS and Tett SFB (1996b) A search for human influences on the thermal structure in the atmosphere. Nature, in press.

Schönwiese CD, Birrong W, Schneider U, Stähle U, and Ullrich R (1990): Statistische Analyse des Zusammenhangs säkularer Klimaschwankungen mit externen Einflußgrößen und Zirkulationsparametern unter besonderer Berück sichtigung des Treibhausproblems. Report No. 84, Institute of Meteorology and Geophysics, University of Frankfurt/M, 260 pp .

von Storch J (1994) Interdecadal variability in a global coupled model, Tellus, 46A, 419-432.

von Storch J , Kharim V, Cubasch U, Hegerl GC, Schriever D, von Storch H and Zorita E (1996): A 1260-year control integration with the coupled ECHAM1/LSG general circulation model. J. Climate, provisionally accepted.

von Storch H and Zwiers FW(1996): Statistical Analysis in Climate Research. Cambridge University Press, in preparation.

Stouffer, R.J., Manabe S, and Vinnikov KYa (1994): Model assessment of the role of natural variability in recent global warming. Nature, 367, 634 - 636.

Tett SFB, Johns TC and Mitchell JFB (1996) Global and regional variability in a coupled AOGCM. Climate Dynamics, provisionally accepted.

Voss R, Sausen R and Cubasch U (1996) Periodically synchronously coupled integrations with the atmosphere-ocean general circulation model ECHAM3/LSG. Part I: Simulations of the present-day climate. In preparation.

Wigley TML and Raper SCB (1990) Natural variability of the climate system and detection of the greenhouse effect. Nature, 344, 324-327.

Figure Legends

Figure 1. Time evolution of global near surface air temperature for experiments C with greenhouse gas forcing only, and two experiments A, B including the aerosol effect, compared with observations (5-year running mean). Temperature changes are defined relative to the mean of the years 1951 to 1980 and are averaged only over areas for which a sufficient number of observations is available and which are used for the detection analysis (cf. Fig. 4).

Figure 2. Change of winter (DJF) mean near surface air temperature in the mean over the decade 2041-2050 relative to the initial decade of the simulations (1880-1889) for the experiments without aerosols (top) and the average of both simulations with aerosols (bottom) [^{o}C].

Figure 3. Same as Figure 2, but for summer (JJA).

Figure 4. Dominant climate change signal (i.e. first EOF) for annual mean data of the greenhouse gas only (a) and the mean of the two combined greenhouse gas and aerosol forcing experiments (b) (normalized to same mean square deviation). The patterns are used as "signal guess-patterns", i.e. anticipated patterns of climate change, for the detection approach. The patterns are restricted to grid-points for which reliable trends could be calculated since 1949 from the observations.

Figure 5. Time evolution of the first 3 EOFs of the mean of both combined forcing simulations. The first EOF picks up most of the monotonous climate change signal, while higher EOFs contain mainly noise.

Figure 6. Optimal fingerprint calculated from the HAML variability data for the combined greenhouse gas and aerosol climate change signal. The optimal fingerprint shows a cooling in the North Atlantic and changed patterns over the large land

masses relative to the climate change pattern (Fig. 4, bottom), but retains the main feature that the warming is weaker in the Northern Hemisphere than in the Southern Hemisphere [normalized in the same way as fig. 4].

Figure 7. Evolution of the detection variable (computed with the optimal fingerprint) for 30-year trend patterns from the observations, the average (A+B)/2 of the simulations A, B and simulation C. The time refers to the final year of the 30-year interval used to compute the trend pattern. 95% confidence intervals derived from three sets of variability data are also indicated. For the present one-tailed test (the signal is known to be positive) the positive confidence limit corresponds to the 97.5% significance level. The recent observed trends exceed this limit, indicating that they represent a significant (at the 97.5% level) climate change. The fingerprint is normalized relative to the standard deviation of the HAML noise, the unit value of the detection variable corresponding to the standard deviation of the HAML noise.

Figure 8. Reduced pattern correlations (with spatial mean subtracted) between observed 30-year trends and the dominant climate change signal (cf. fig. 4) for the averaged simulations A, B (greenhouse gas + aerosols; full line) and for simulation C (greenhouse gas only; dashed line).

Figure 9. a) Orthogonal pattern (relative to the Euclidean metric) to the greenhouse warming signal pattern, b) optimal fingerprint for the statistically orthogonal signal pattern (relative to the covariance matrix metric). Both represent the additional climate change pattern which has been introduced by the aerosol forcing assuming a linear superposition principle [normalized in the same way as fig. 4].

Figure 10. a) Evolution of the observed temperature trends in a phase space spanned by the detection variable using the signal pattern for greenhouse warming (1) and the statistically orthogonal signal pattern representing the aerosol effect (2; the

optimized orthogonal fingerprint is shown in Figure 9b). The detection variable for trend patterns ending in different time intervals are shown in different colors, selected trends are additionally marked in the figure. The arrows show the time evolution. b) shows the results for the observations compared to the detection variable computed with 30-year trend patterns from various data of climate variability. Additionally, the ellipses containing 95% of the estimated Gaussian distribution for these climate variability data are shown. Note the different shape of the noise ellipses for different variability data.

Figure 11. Attribution diagram for 30-year annual mean trends. The phase space is the same as in fig. 10. The detection variables for the 30-year trend pattern 1966-1995 in the model simulations are shown by the colored dots. Since the underlying model climate change signal is expected to agree with the dominant signal pattern (Fig. 4), these dots are projected onto it, yielding the amplitude estimates of the simulated climate change patterns ("X"). The ellipses centered around these "X" values indicate the 90% confidence areas for each simulation. They have been computed from the uncertainty associated with a single or only two model simulations and additional climate noise present in the observations (using the HADCM2 noise). Since two simulations A,B are used for the combined forcing signal amplitude, the uncertainty is reduced (as indicated by the smaller ellipse). The detection variable for the latest observed 30-year trend lies inside the confidence ellipse for the combined forcing signal, but outside the confidence ellipse of the greenhouse gas only signal. Thus the observations are inconsistent (but only marginally) with a pure greenhouse gas forced climate change signal and agree with a combined forcing climate change signal.

Figure 12. Observed pattern of 50-year trends for the period 1946 -1995 in summer (JJA) (^{0}C/Decade], calculated from the data of Jones and Briffa.

Figure 13. a) Evolution of 50-year summer trends in a phase space spanned by the detection variable for greenhouse gas only and combined forcing signal patterns together with different estimates for climate variability (cf. fig. 10b) and the respective 95% confidence ellipses. b) Attribution diagram for 50-year trends in summer, notation similar to figure 11. The latest observed 50-year trends lie outside the 95% confidence ellipse for a greenhouse gas only signal. Thus we conclude that they are inconsistent (at a more than 95% confidence level) with a pure greenhouse gas signal. On the other hand, the observations are consistent with a combined forcing climate change signal.

Table 1: Estimates of the signal-to-noise ratio for the latest observed annual mean near surface temperature trend using different fingerprints, namely 1) "mean": a uniform fingerprint yielding the global mean as detection variable; 2) "non- opt": the signal guess-pattern, and 3) "opt": the optimal fingerprint. Also listed are the improvements in the signal-to-noise ratios through use of "non-opt" relative to "mean" and "opt" relative to "non-opt". Different columns depict the estimates derived from different variability data: the control simulations HAML, HAM3L, GFDL, HADCM2, and the observations with a previously estimated anthropogenic greenhouse gas value subtracted (VOBS) and fro, 1860-1960 without subtraction of the greenhouse gas component (ROBS). The optimization is performed in a space which is truncated to the first 10 EOFs of simulation A. Here and in the following tables the signal-to-noise ratios using the optimal fingerprint for HAML are given in parentheses, since these have a positive bias due to the use of the same data for the optimization. Bold numbers indicate that the results are significant at the 97.5% level. An asterisk (*) denotes a decrease in signal-to-noise ratio due to optimization, indicating problems in the optimization (cf. Section 5)

	HAML	HAM3 L	GFDL	HADC M2	VOBS	ROBS
mean	6.00	**5.14**	**4.28**	**3.21**	**3.01**	**2.58**
non-opt	5.92	**5.66**	**4.57**	**3.35**	**3.15**	**2.71**
opt	(6.92)	**4.87***	**4.47***	**4.36**	**3.28**	**2.81**
Improvement:						
non-opt / mean	0%	8%	7%	4%	5%	5%
opt / non-opt	(17%)	-20%	-2%	30%	4%	4%

Table 2: Estimates of the signal-to-noise ratio of the detection variable d2 computed with the orthogonal pattern introduced by the aerosol forcing in addition to the greenhouse gas forcing (fig. 9). c_2/c_1 denotes the ratio of the contributions from the orthogonal aerosol response pattern and the pure greenhouse gas response pattern to the model simulated greenhouse gas + aerosol climate change pattern (cf. equ. 11). Notation otherwise as in Table 1.

	c_2/c_1	HAML	HAM3 L	GFDL	HADC M2	VOBS
non-opt:	0.32	0.80	0.49	1.09	0.56	0.87
opt:	0.31	(2.32)	1.48	***2.60***	1.67	***2.16***

Table 3: Signal-to-noise estimates for the lastest observed trend based on the non-optimized and optimized combined forcing fingerprint for seasonal data. α denotes the (mean included) correlation between the non-optimized and optimized fingerprint, otherwise notations like in Table 1. A decrease in signal-to-noise ratio after optimization (indicated by the asterisk) suggests either differences in the structure of variability in different models or an incorrect signal pattern.

	α	HAML	HAM3L	GFDL	HADCM2
WI: non-opt		**5.41**	**4.31**	**4.45**	**4.00**
opt	0.79	**(4.88*)**	**3.25***	**3.77***	**3.09***
SP: non-opt		**5.86**	**5.55**	**4.58**	**3.38**
opt	0.87	**(5.53*)**	**4.03***	**3.93***	**2.95***
SU: non-opt		**5.59**	**4.73**	**3.42**	**2.90**
opt	0.92	**(5.81)**	**4.18***	**3.35***	**3.40**
AU: non-opt		**4.59**	**3.61**	**2.99**	**2.31**
opt	0.91	**(4.98)**	**3.49***	**3.24**	**2.45**

Table 4: Same as Table 2, but for 50-year observed temperature trends of summer data. All data have been truncated to a 6-dimensional space (as opposed to the 10-dimensional used for 30-year trends, where more independent data from a 1000-year simulation are available). The contribution of the aerosol pattern is larger than expected from noise in all cases, at the 90 (95)% confidence level for the values printed in italics (bold italics).

Summer, 50yr.	c_2/c_1	HAML	HAM3L	GFDL	HADCM2
non-optimized	0.50	***3.89***	***2.25***	***3.64***	*1.98*
optimized	0.63	***4.49***	***2.86***	***4.22***	***2.53***

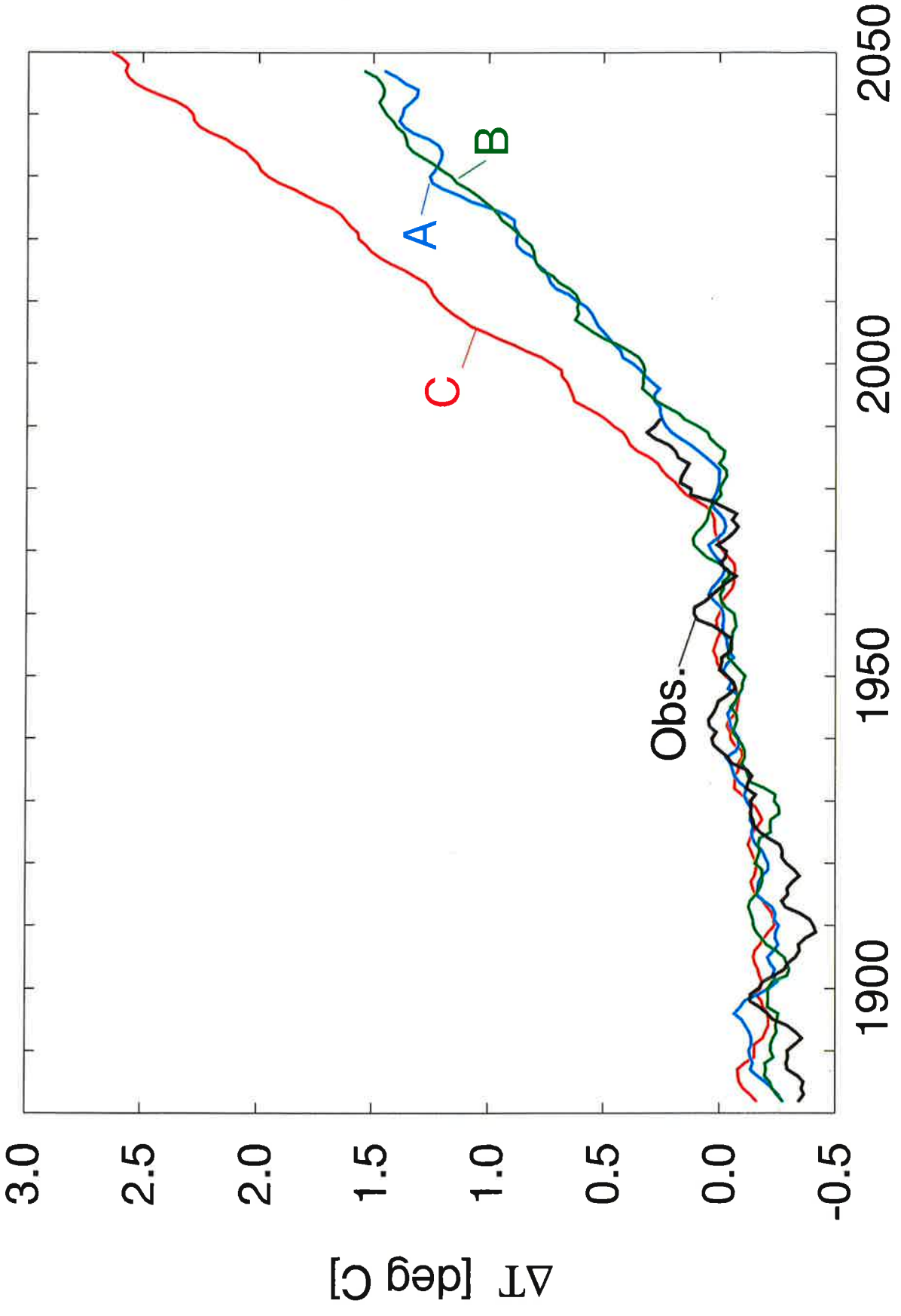

Figure 1

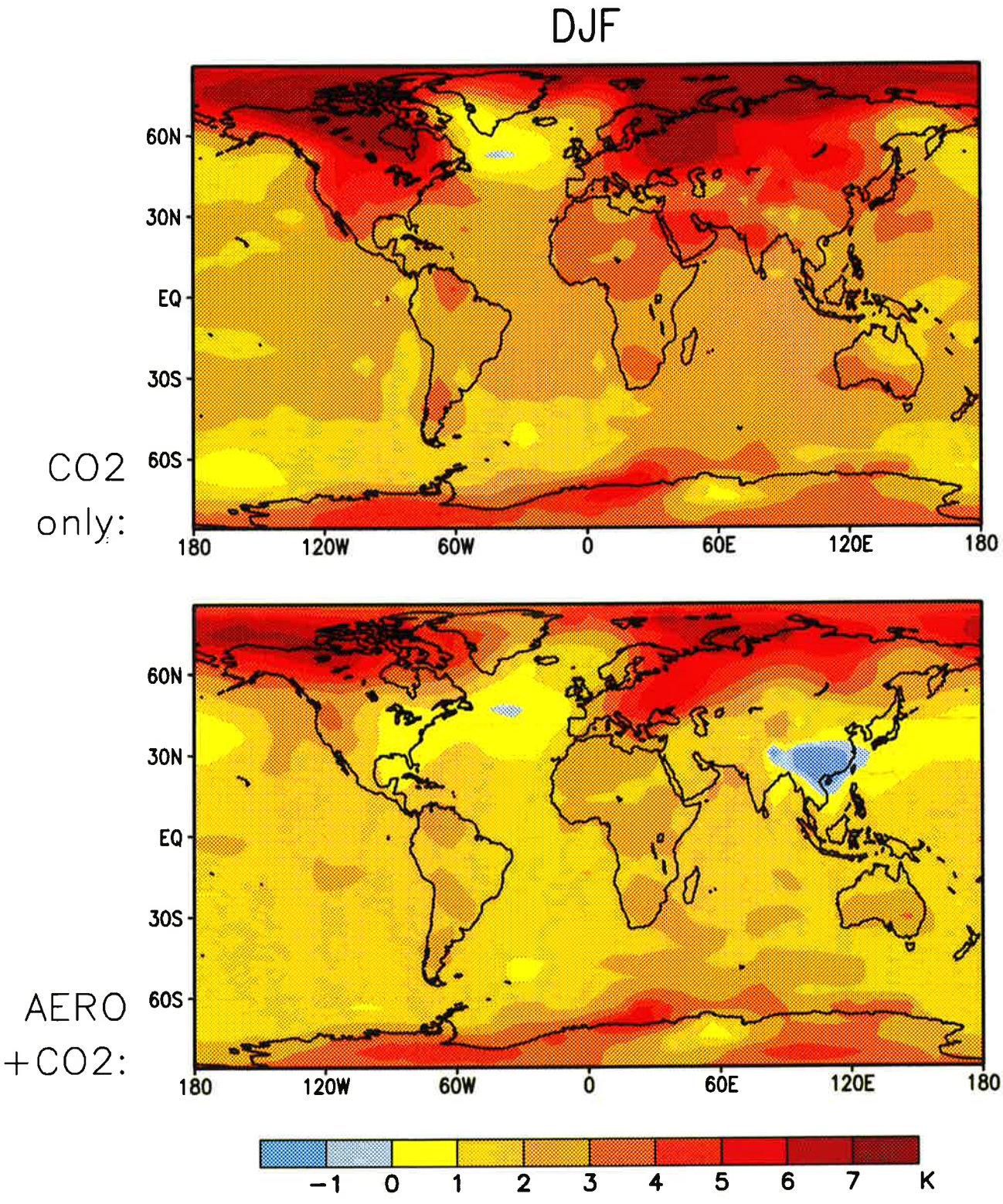
DJF
CO2
only:
AERO
+CO2:
60N
30N
EQ
30S
60S
180
120W
60W
0
60E
120E
180
−1
0
1
2
3
4
5
6
7
K

Figure 2

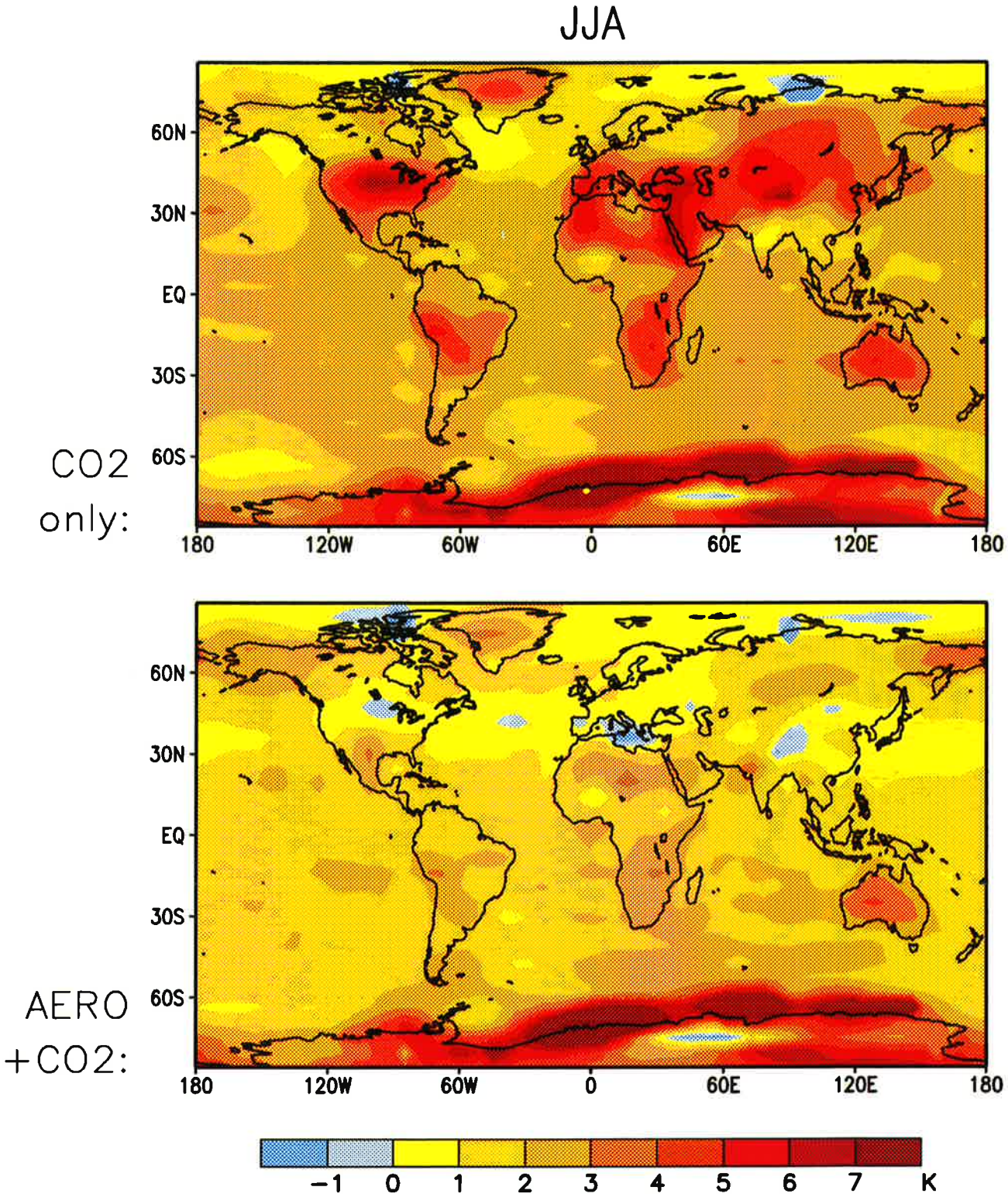
JJA
CO2
only:
AERO
+CO2:
60N
30N
EQ
30S
60S
180
120W
60W
0
60E
120E
180
−1
0
1
2
3
4
5
6
7
K

Figure 3

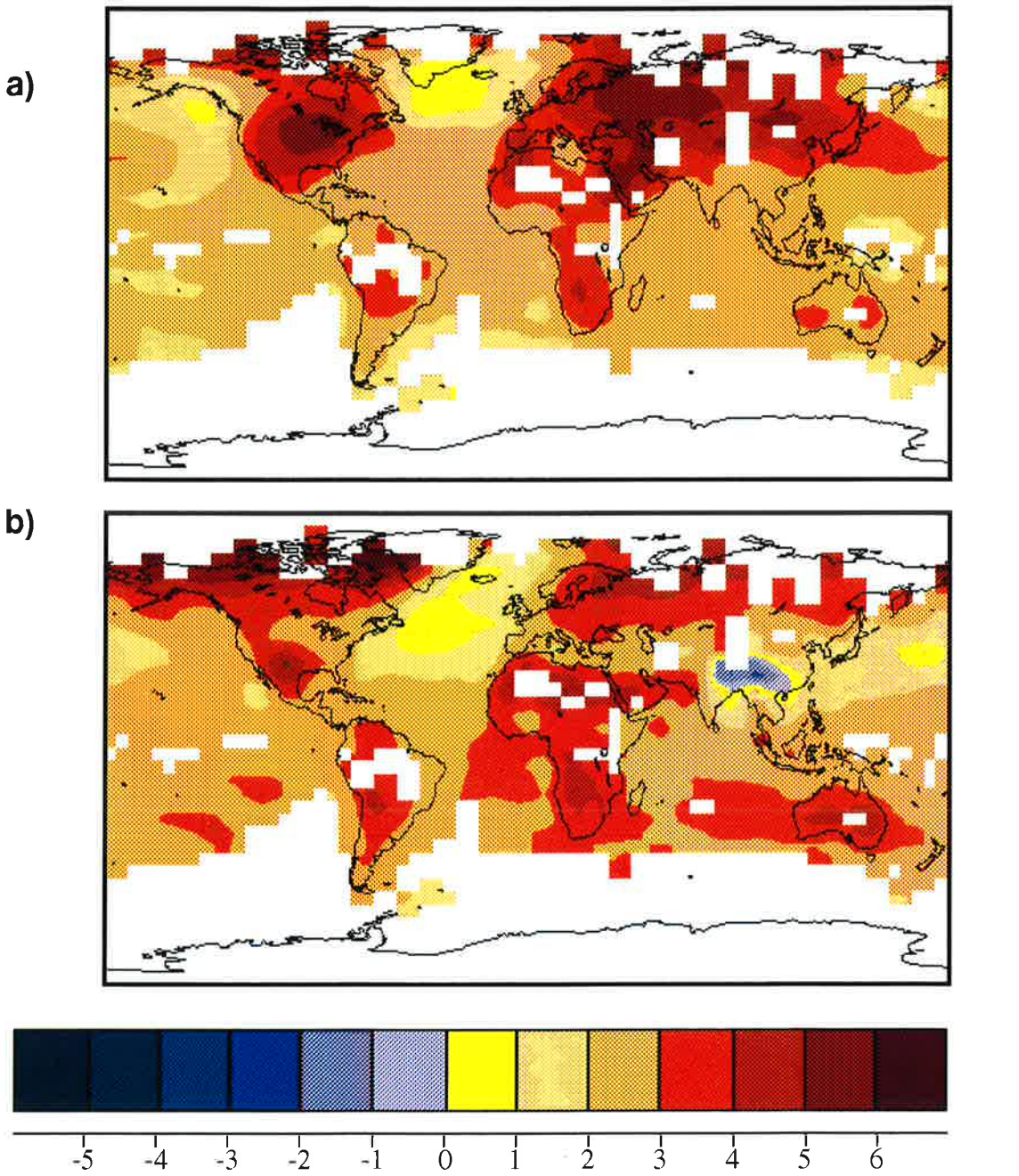

Figure 4

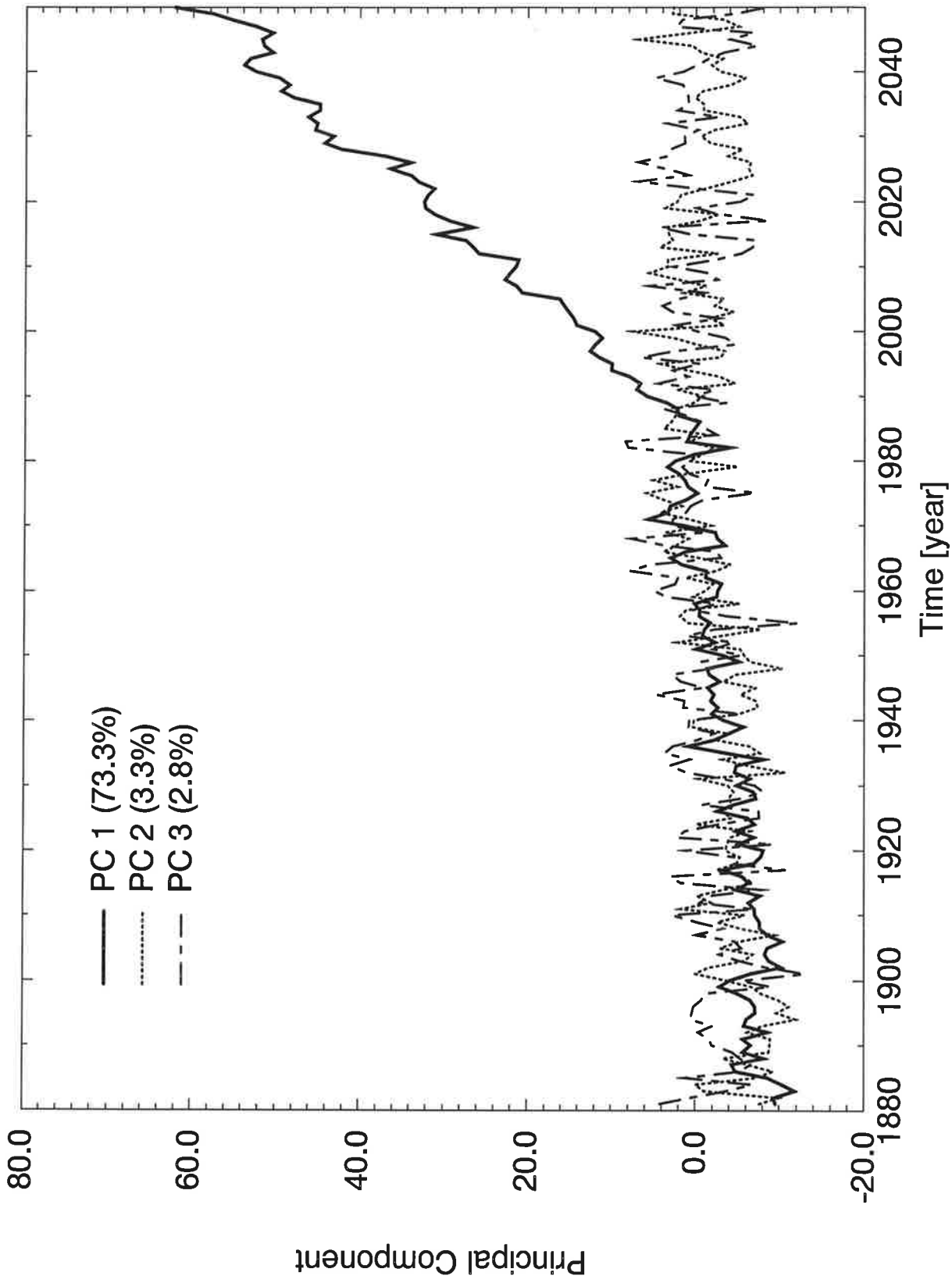
PC 1 (73.3%)
PC 2 (3.3%)
PC 3 (2.8%)
80.0
60.0
40.0
20.0
0.0
-20.0
1880
1900
1920
1940
1960
1980
2000
2020
2040
Time [year]
Principal Component

Figure 5

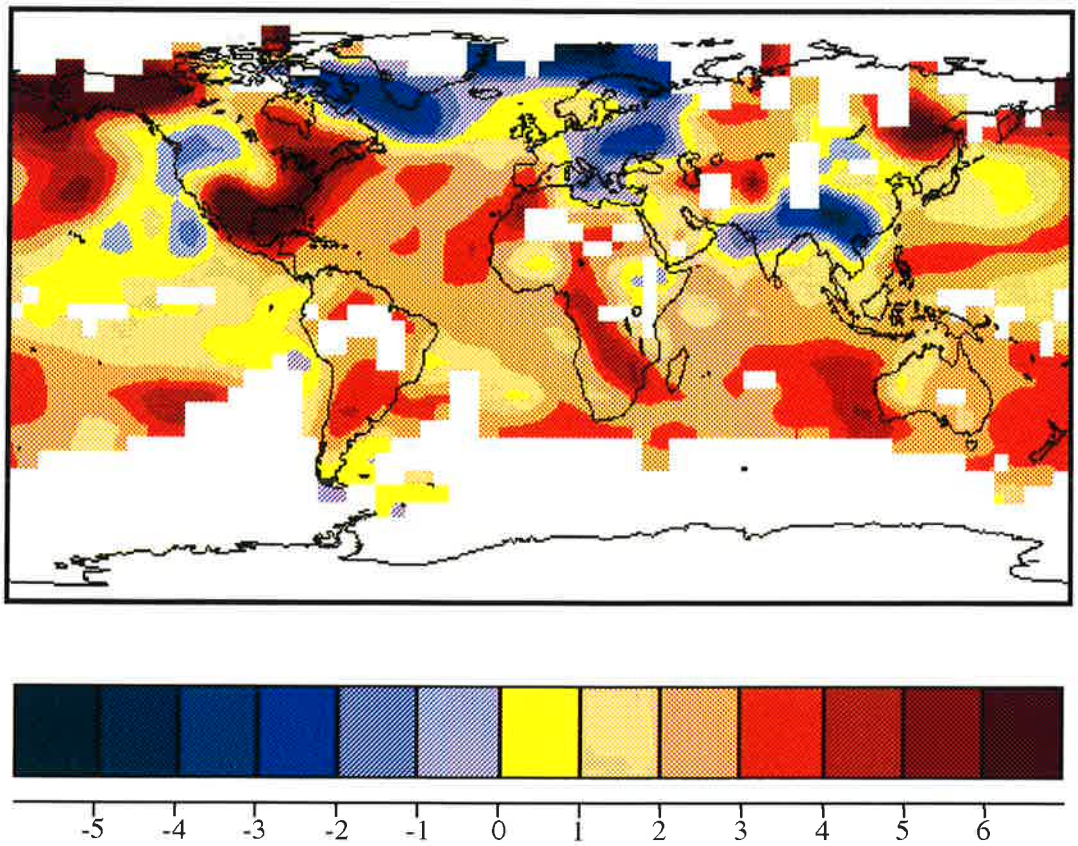

Figure 6

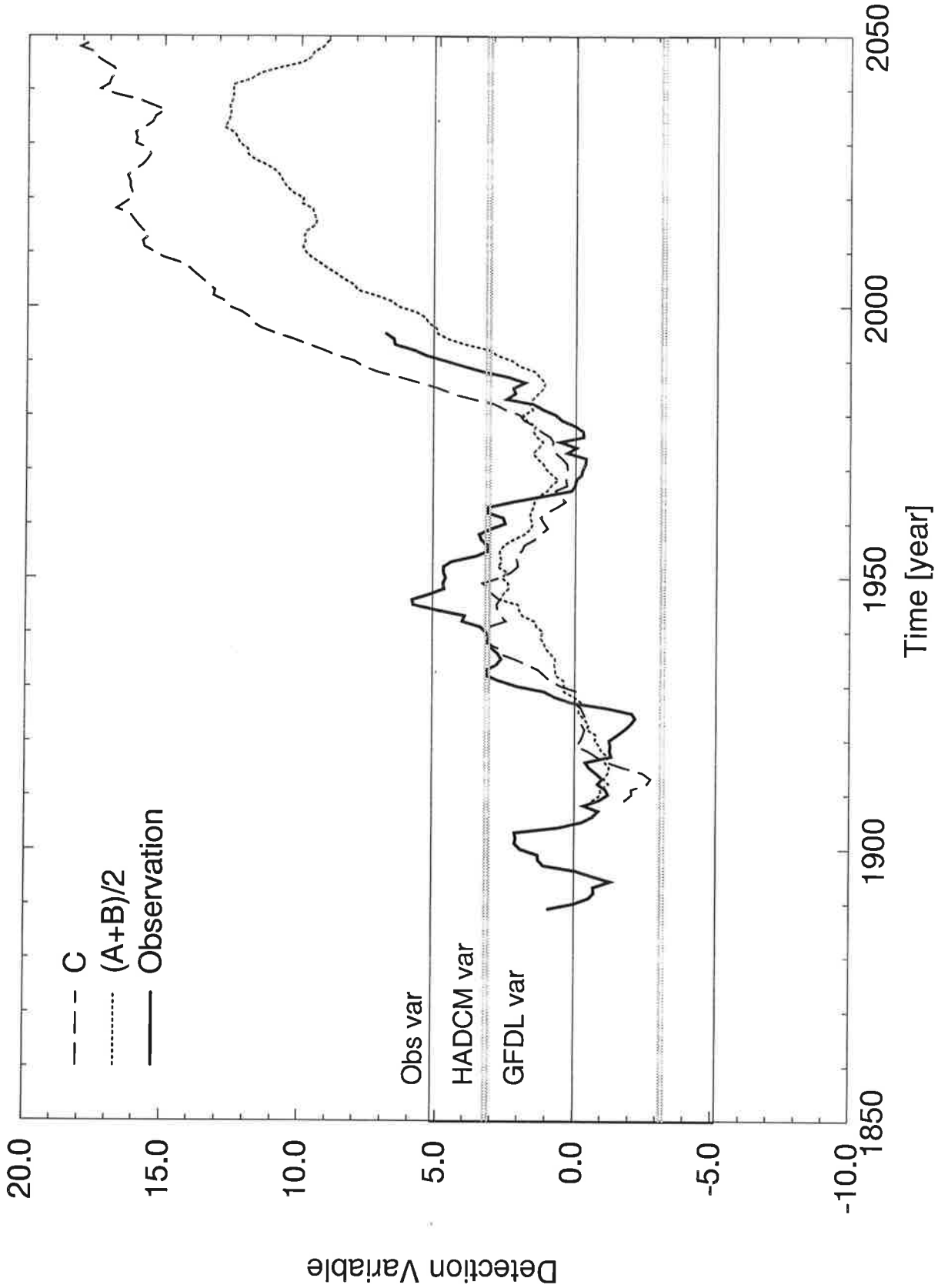
C
(A+B)/2
Observation
Obs var
HADCM var
GFDL var
20.0
15.0
10.0
5.0
0.0
-5.0
-10.0
1850
1900
1950
2000
2050
Time [year]
Detection Variable

Figure 7

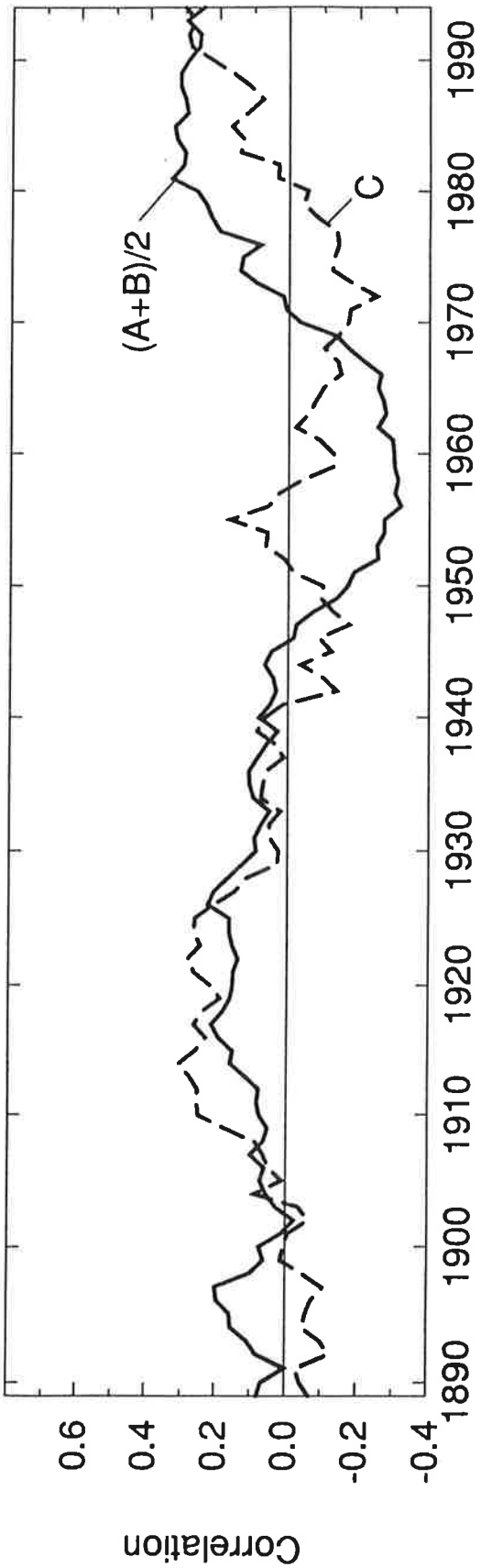
(A+B)/2
C
Correlation
0.6
0.4
0.2
0.0
-0.2
-0.4
1890
1900
1910
1920
1930
1940
1950
1960
1970
1980
1990

Figure 8

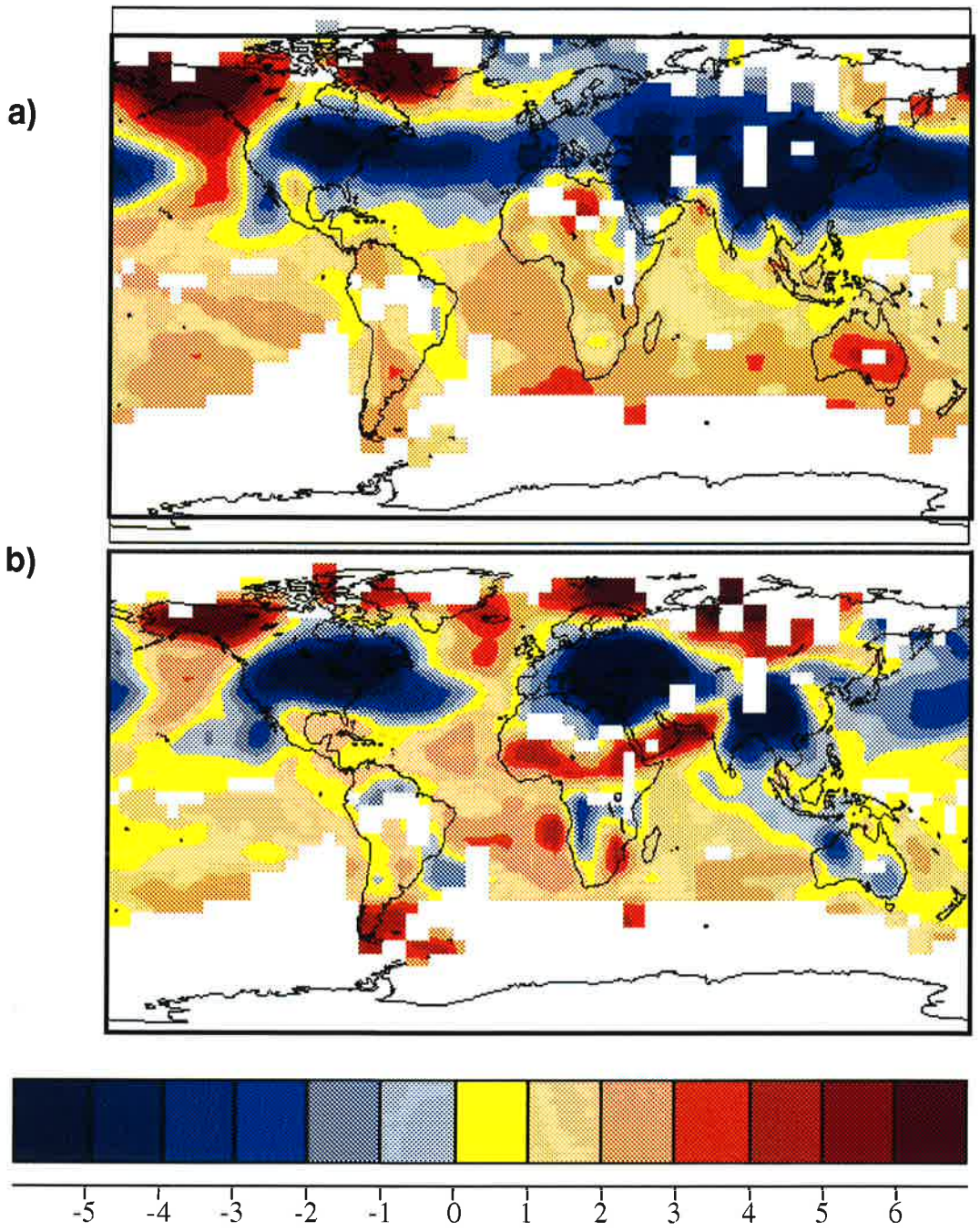

Figure 9

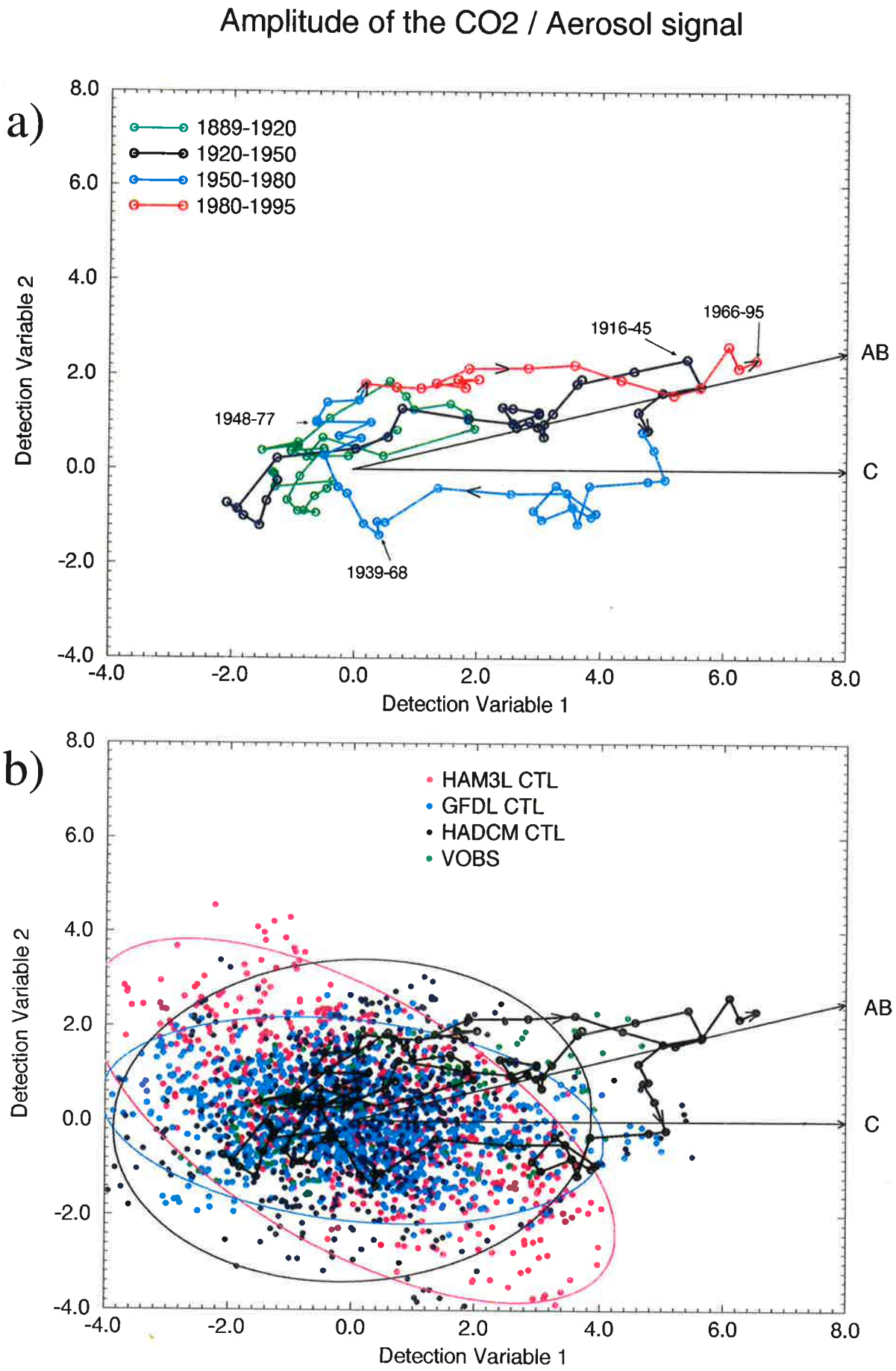
Amplitude of the CO2 / Aerosol signal
a)
1889-1920
1920-1950
1950-1980
1980-1995
1916-45
1966-95
1948-77
1939-68
AB
C
Detection Variable 2
Detection Variable 1
8.0
6.0
4.0
2.0
0.0
-2.0
-4.0
b)
HAM3L CTL
GFDL CTL
HADCM CTL
VOBS
AB
C
Detection Variable 2
Detection Variable 1

Figure 10

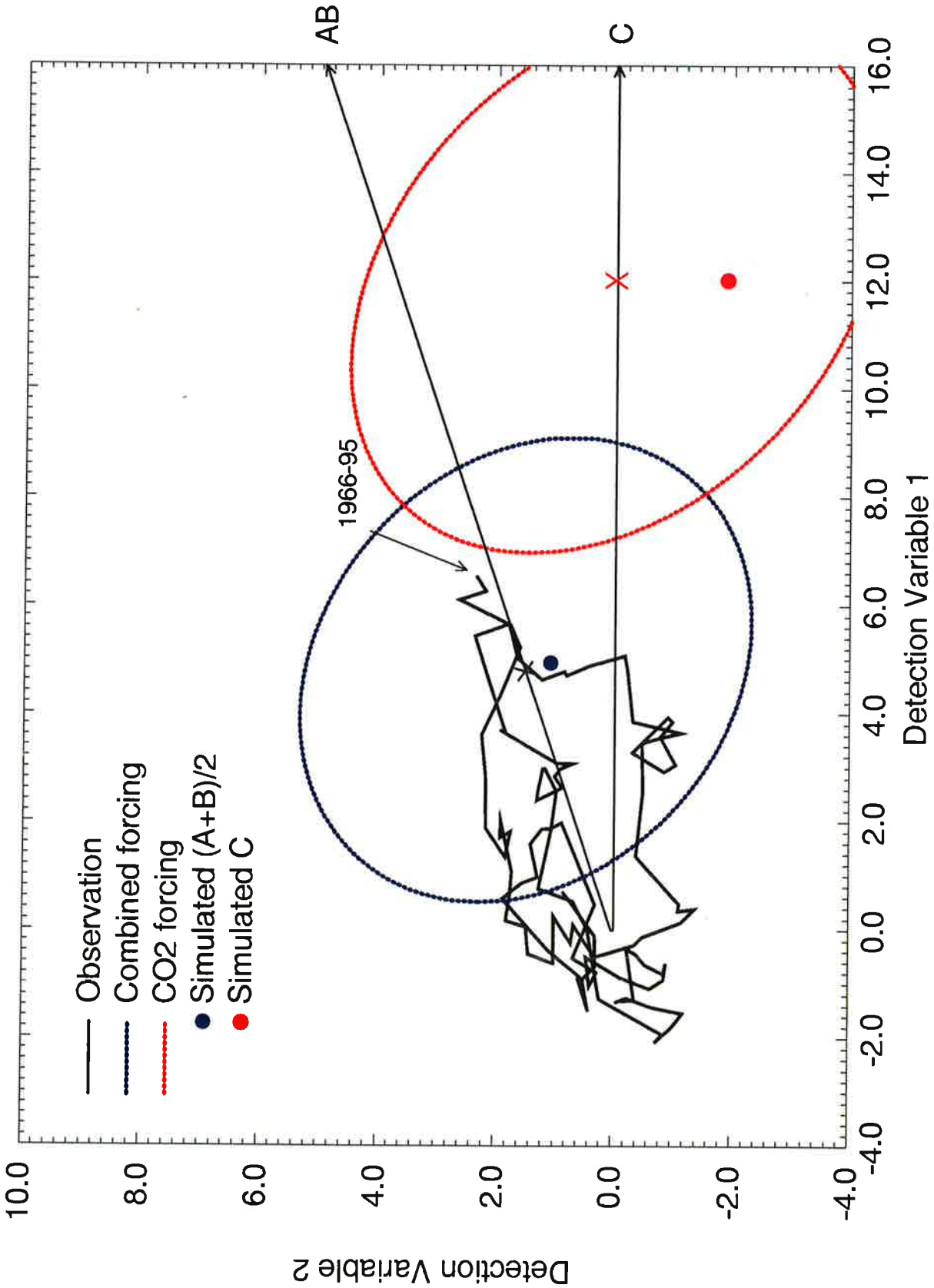
AB
C
1966-95
Observation
Combined forcing
CO2 forcing
Simulated (A+B)/2
Simulated C
Detection Variable 1
Detection Variable 2
16.0
14.0
12.0
10.0
8.0
6.0
4.0
2.0
0.0
-2.0
-4.0
10.0
8.0
6.0
4.0
2.0
0.0
-2.0
-4.0

Figure 11

Observed 50-Year Summer Trends: 1946-1995

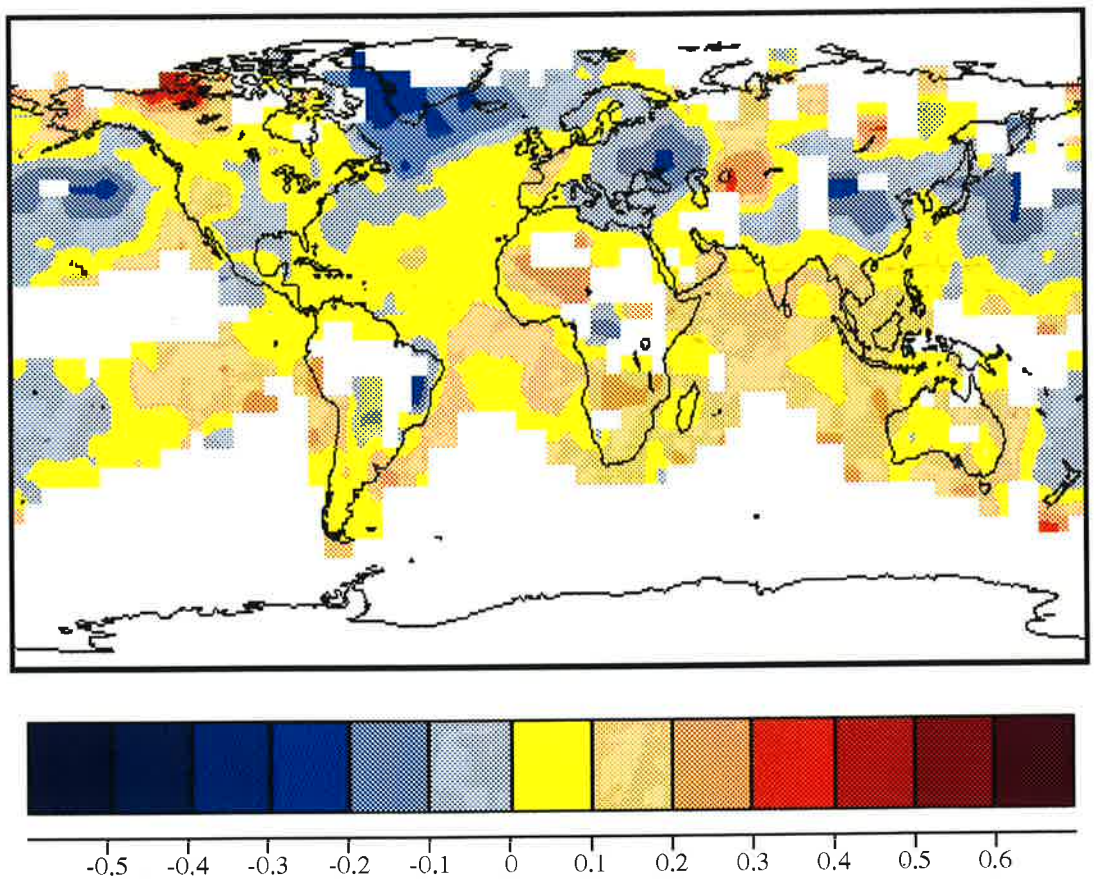

Figure 12

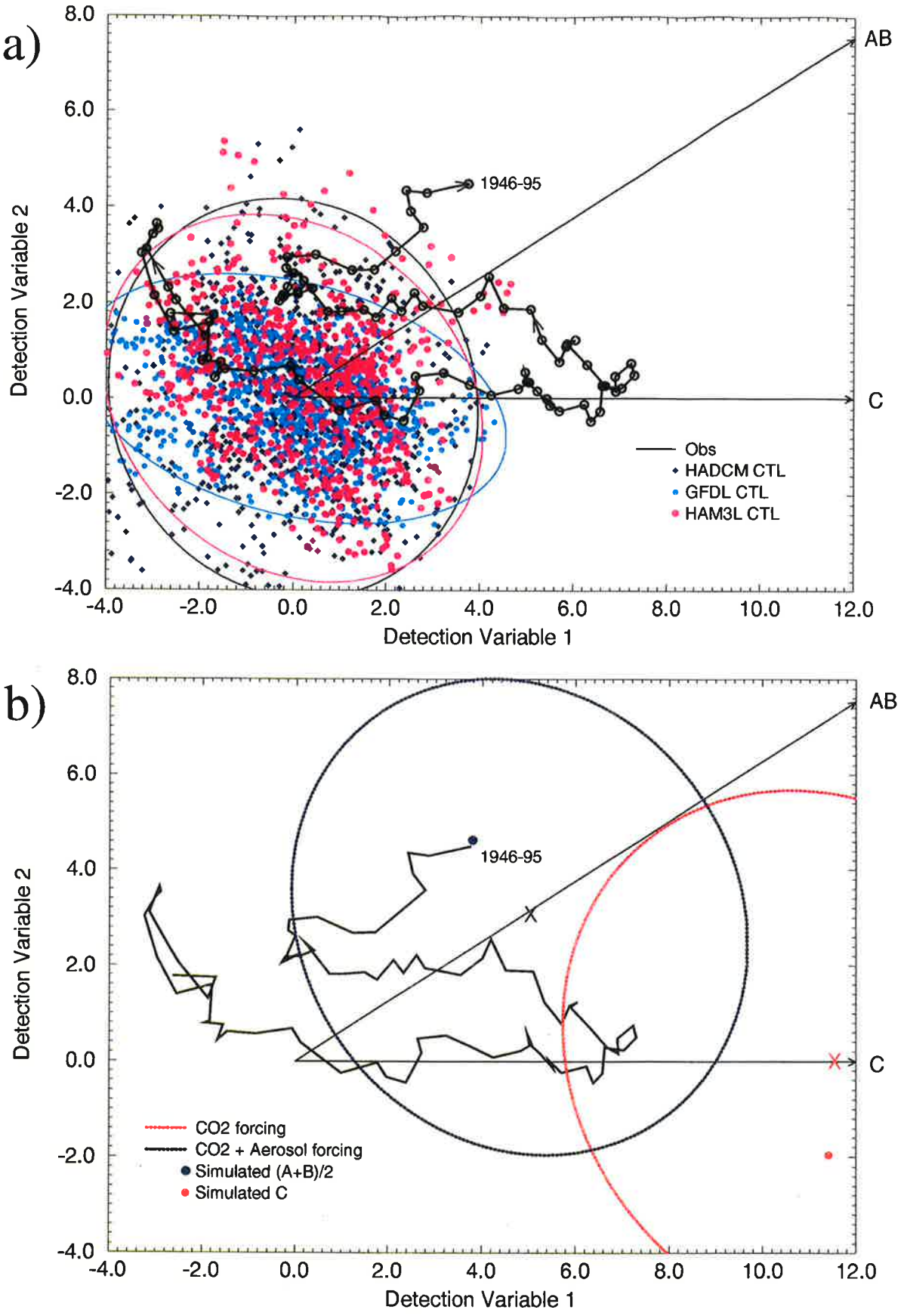
a)
AB
C
1946-95
Obs
HADCM CTL
GFDL CTL
HAM3L CTL
Detection Variable 2
Detection Variable 1
8.0
6.0
4.0
2.0
0.0
-2.0
-4.0
-4.0
-2.0
0.0
2.0
4.0
6.0
8.0
10.0
12.0
b)
AB
C
1946-95
CO2 forcing
CO2 + Aerosol forcing
Simulated (A+B)/2
Simulated C
Detection Variable 2
Detection Variable 1

Figure 13